applied sciences

MDPI

Article

Comprehensive Six-Degrees-of-Freedom Trajectory Design and Optimization of a Launch Vehicle with a Hybrid Last Stage Using the PSO Algorithm

Ukte Aksen [1,2,*], Alim Rustem Aslan [1] and Umit Deniz Goker [3]

[1] Department of Astronautical Engineering of Aeronautics and Astronautics, Istanbul Technical University, 34485 Istanbul, Turkey; aslanr@itu.edu.tr
[2] Microelectronic Guidance and Electro-Optical Group, Aselsan Inc., 06200 Ankara, Turkey
[3] Department of Solar Physics, Astronomical Institute of Czech Academy of Sciences, Fričova 298, 251 65 Ondřejov, Czech Republic; deniz.umit.goker@asu.cas.cz
* Correspondence: oneru@itu.edu.tr or uaksen@aselsan.com

Abstract: Increased performance with reduced overall cost, and precise design and optimization of launch systems are critical to affordability. In this respect, the use of hybrid motors has increased to ease handling based on motor selection. In the current study, the launch vehicle's performance is enhanced by incorporating a hybrid rocket motor into the last stage and optimized using particle swarm optimization to develop a six-degrees-of-freedom tool. This modification aims to increase payload placement flexibility, facilitate handling, and reduce costs. Thanks to the interactive subsystems within this research, this innovative study more comprehensively considers the launch vehicle trajectory design problem, allowing the simultaneous consideration of the effect of launch vehicle geometry along with other parameters in the system. In this context, the proposed method is applied to the Minotaur-I launch vehicle, and contributions of the detailed design and optimization are presented. Optimization results show that the percentage differences between these models for the original vehicle were observed to be 11.55% in velocity and 8.02% in altitude. However, there were differences of 10.06% and 48.8%, 15.8% and 23.2%, and 19.5% and 78.9% in altitudes and velocities when the center of gravity and moment of inertia changes were neglected, and constant aerodynamic coefficients were assumed, respectively. In all these cases, it was observed that the flight path angle was not close to zero. Moreover, the same mission was achieved by the launch vehicle with the optimized hybrid last stage and the propulsion performance was increased by about 7.64% based on the specific impulse and total impulse-over-weight ratio.

Keywords: hybrid rocket motors; launch vehicles; particle swarm optimization; multidisciplinary optimization

check for updates

Citation: Aksen, U.; Aslan, A.R.; Goker, U.D. Comprehensive Six-Degrees-of-Freedom Trajectory Design and Optimization of a Launch Vehicle with a Hybrid Last Stage Using the PSO Algorithm. *Appl. Sci.* **2024**, *14*, 3891. https://doi.org/10.3390/app14093891

Academic Editor: Yan Wang

Received: 15 April 2024
Revised: 28 April 2024
Accepted: 28 April 2024
Published: 1 May 2024

1. Introduction

Since the beginning of the space race, a variety of launch vehicles have been developed to transport a satellite to Earth's orbit or beyond, astronauts to the Moon, or scientific instruments and cargo to the International Space Station. Launch vehicles or launchers can be classified according to their mass capabilities such as heavy-lift, medium-lift, and small-lift, while ballistic missiles have been transformed into space launch vehicles; for example, Delta IV from the heavy-lift launch vehicle category was derived from the Thor intermediate-range ballistic missile, which was the first operational ballistic missile of the United States Air Force (USAF); and the small-lift Falcon-9 was derived from many of today's launch vehicles to avoid the cost and simplify the design process [1]. Traditionally, small satellites and light-weight satellites have been launched into space as secondary payloads on larger launch vehicles. However, the secondary payload approach did not provide specific requirements such as launch timing and orbital characteristics for many small satellites. Therefore, smaller launch vehicles for a wide range of applications for small satellite missions have been started to be developed.

With the increased number of small satellites developed and launched yearly, there has been a strong need to reduce launch costs and lower handling and preparation times. HRM stands out as a strong candidate to meet these needs with advantages such as increased safety, throttle control, environmentally friendly propellants, simplified design, cost-effectiveness, combustion efficiency, ease of testing and handling, and potential for reusable components, making them attractive for specific applications. Several pioneering companies have been at the forefront of advancing hybrid rocket propulsion technology, fusing the advantages of both solid and liquid propulsion methods. Virgin Galactic, renowned for its suborbital space tourism endeavors, has also delved into hybrid rocket technology for its SpaceShipTwo suborbital spacecraft [2]. Notably, ARCA Space Corporation has been working diligently on hybrid rocket technology with aspirations to create launch vehicles and spacecraft capable of deploying payloads to various orbits [3]. Beyond these, ExPace, a subsidiary of China Aerospace Science and Industry Corporation (CASIC), has made strides in the hybrid propulsion sector, particularly with the Kuaizhou series of rockets, contributing to China's space endeavors [4]. Additionally, Nammo, a European aerospace and defense company, has demonstrated commitment to hybrid rocket technology, joining the ranks of innovative entities aiming to revolutionize propulsion in both civil and military applications [5]. The HANBIT-TLV suborbital rocket serves as a precursor to the company's upcoming commercial satellite launcher, the Hanbit-Nano [6]. This two-stage small satellite launcher is meticulously designed to transport payloads weighing up to 50 kg to a 500 km sun-synchronous orbit. These companies, among others, symbolize cutting-edge progress in hybrid rocket propulsion, which has domain-rich potential to transform space access and exploration paradigms.

The results from a comparison of the advantages and disadvantages of SRMs, LRMs, and HRMs shown in Table 1. Articles by Schoettle and Hillesheimer (1991), Lu and Pan (1992), Eberhart and Shi (1998), Gath and Calise (2001), Miele (2002), Miele (2003), Venter and Sobieszczanski-Sobieski (2003), Bayley (2007), Rafique et al. (2009), Kitagava et al. (2012), DaLin et al. (2012), Pontani (2014), Dileep et al. (2015), Wiegand et al. (2015), Zhou et al. (2017), Lappas (2019), Casalino et al. (2022), Mall and Taheri (2022), and Villanueva (2022) present very detailed studies on HRMs and their historical developments. HRMs have been extensively studied due to their unique design combining solid and liquid propulsion elements [7–27]. Their historical development spans decades, with significant advancements in understanding combustion dynamics, performance optimization, and safety enhancements. These studies have contributed to the broader field of rocket propulsion, offering innovative solutions and insights into efficient and reliable space propulsion technologies. In Table 1, the items indicated with a "+" sign on the table represent advantages, those with a "−" sign indicate disadvantages, and "N/A" signifies the absence of either advantages or disadvantages.

According to Table 1, solid rocket propulsion offers advantages in simplicity and reliability due to minimal moving parts, featuring stable propellants ideal for extended storage and fixed thrust profiles as seen in boosters. However, a drawback is their lack of throttle control, impeding precise adjustments, and once ignited, they are not easily shut down. This contrasts with liquid propulsion, which provides precise throttle control and restart capabilities for intricate missions like orbital maneuvers. Liquid propellants enhance fuel efficiency and performance with high specific impulse allowing for a variety of propellant combinations. Nonetheless, the complexity of liquid motors leads to increased manufacturing and maintenance costs, and volatile propellants demand cautious handling due to potential degradation. On another point, hybrid propulsion amalgamates solid safety with liquid control, excelling in throttle adaptability and potentially higher efficiency, and some hybrid propellants are environmentally friendlier.

Table 1. Comparison of advantages and disadvantages of solid, liquid, and hybrid rocket motors.

Properties	Solid	Liquid	Hybrid
Simplicity	+	−	−
Reliability	+	N/A	+
Storage	+	−	N/A
Thrust	High	N/A	Limited
Operational Flexibility	+	−	+
Controllability	−	+	N/A
Restart Capability	−	+	+
Specific Impulse	Low	High	N/A
Safety	N/A	−	+
Cost-effectiveness	N/A	N/A	+
Grain Robustness	N/A	N/A	+
Eco-friendly	N/A	N/A	+
Performance	N/A	N/A	+

The superior density-specific impulse ($\rho - I_{sp}$) values exhibited by solid propellants render them highly suitable for deployment in compact stages, which are particularly well-suited for the initial phases of a launch vehicle. Their inherent reliability, devoid of the need for pumps and valves, is a noteworthy characteristic [7]. However, this commendable performance and shutoff control capability may not extend effectively to upper stages due to the limitations associated with lower I_{sp} of around 210–250 s. In contrast, liquid rocket motors (LRMs) circumvent these challenges by offering higher I_{sp} and the added advantage of flexible stop-and-restart capabilities. Typically, liquid oxygen (LOX) serves as the oxidizer (O), while either liquid hydrogen (LH2) or RP-1 functions as the fuel (F), influencing propellant performance significantly [3]. Hybrid rocket motors (HRMs) share performance similarities with storable or semicryo LRMs. With oxygen (Ox) stored separately from F, HRMs boast the ability to be shut off and restarted akin to LRMs, along with the capacity for throttling within a broad thrust (T) range [3]. Combining advantageous features of both solid rocket motors (SRMs) and LRMs, HRMs have garnered considerable attention in contemporary technologies, primarily due to their merits in terms of high safety, simplicity, cost-effectiveness, stop-and-restart capability, throttling ability, and the utilization of environmentally friendly propellant combinations. Despite these advantages, HRMs exhibit certain drawbacks, including a low solid F regression rate and intricacies related to the coupling between mixture-ratio values and thrust levels. Notwithstanding these issues, the successful utilization of HRMs in SpaceShipOne, marking the first private manned space flight, underscores their potential and applicability [4]. The distinctive characteristics of HRMs, such as the separate storage of solid and liquid oxidizers, contribute to enhanced safety and cost-effectiveness throughout the manufacturing, storage, transportation, and operational processes [10]. The specified features indicate that HRMs are advantageous compared to solid and liquid rocket motors, and the importance of their use is highlighted in conjunction with evolving technology. Considering these attributes, it is posited that the integration of HRMs as a stage of a launch vehicle can significantly enhance the overall performance of launch vehicles.

The historical dominance of solid and liquid propulsion in space exploration has resulted in a wealth of knowledge and established technologies, creating a gravitational pull towards these proven systems. The preferences and investments of the space industry, including governmental space agencies and private companies, can strongly influence research priorities, with a bias towards traditional technologies. Additionally, the perception of higher risk and less maturity associated with hybrid rocket technology, especially in multi-stage setups, may make researchers and funding agencies more risk-averse. The limited operational examples of multi-stage launch vehicles utilizing hybrid rocket motors further contribute to a hesitancy among researchers and engineers to delve into this less-traveled domain. Despite these challenges, the dynamic nature of the rocket propulsion environment indicates that research interests are shifting and a focus on hybrid rocket motors has begun, as technologies advance, the industry needs to evolve, and early adopters demonstrate success in the field of hybrid propulsion for multi-stage launch vehicles [11]. Therefore, the optimization studies conducted for multi-stage launch vehicles in the literature are quite limited due to the complexities they entail. Specifically, the number of publications on hybrid rocket motors used in multi-stage launch vehicles is significantly less compared to those on solid- and liquid-fueled rockets [11]. Among the challenges encountered in these studies, obtaining high I_{sp} over a minimum of 280 s is deemed most critical. Some examples of the optimization problem objectives studied are payload maximization, gross lift-off weight (GLOW) minimization, and F consumption minimization [12–14]. The studies discussed trajectory optimization and guidance methods for an advanced launch system, likely focusing on techniques to optimize the path and control of launch vehicle trajectories, as well as the optimization of launch vehicle ascent trajectories under path constraints and coast arcs, exploring methods to enhance the efficiency and performance of launch trajectories. In order to solve these optimization problems, there is a variety of solution methods. For example, genetic algorithms (GAs) have mostly been used to obtain orbit, vehicle weight, stage length (L^*), and total cost [15,16]. This approach leverages computational methods to efficiently explore and refine design variables, contributing to the development of more efficient and cost-effective launch systems. Researchers continue to refine and combine optimization techniques like GA with other algorithms such as sequential quadratic programming (SQP) to further enhance trajectory design and performance across various phases of flight. The SQP method is used by many researchers to find the flight path, motor characteristics, and maximum angle of attack (α) [17–20]. These interdisciplinary approaches underscore the importance of computational optimization in advancing the precision and effectiveness of launch vehicle design and operations. The uniform trigonometrization method (UTM) has been used to optimize the re-entry trajectory of reusable launch vehicles, and SRM characteristics and trajectory are optimized using a hybrid method that combines GA and SQP methods [21,22].

In the last decades, the particle swarm optimization (PSO) technique, which is also a class of heuristic methodology, has become prominent. Simplicity is the main reason for using a swarm algorithm (SA). Because the basic version of the PSO appears very intuitive, it is considerably easier to program and implement. Although it is computationally expensive in comparison with gradient-based methods, in the literature it is reported as being more efficient than GAs because of the decreased number of function evaluations [23,24]. The adoption and further exploration of the PSO in various fields highlight its potential for addressing complex optimization challenges. As researchers continue to refine and adapt PSO techniques to specific application domains, its versatility and effectiveness are likely to be more widely recognized and integrated into diverse optimization problems in the future. Despite its promising features, few researchers have concentrated on PSO to use it in launch vehicle design optimization problems [25–27]. These studies collectively investigate the application of the PSO to optimize ascent trajectories of multi-stage launch vehicles, including addressing ascent phase trajectory optimization problems and enhancing trajectories for vehicles equipped with multi-combined cycle engines. Each of these studies delves into the application of the PSO in optimizing launch vehicle trajectories for different purposes.

In this study, the optimization objective is the determination of hybrid motor characteristics and some flight path parameters such as thrust vector control (TVC) angle to obtain a target trajectory for a specified payload mass (PM). To accomplish this task, the nonlinear coupling between aerodynamics, propulsion, structure, and trajectory subsystems is considered in the six-degrees-of-freedom (6DOF) simulation. Aerodynamic coefficients and structural properties are modeled using Data Compendium (DATCOM) v2011 and Computer-Aided Three-Dimensional Interactive Application (CATIA) V5R19, respectively. The method was applied to the Minotaur-I launch vehicle. Reference is made to the Minotaur-I launch vehicle, which has a total of four stages as solid, e.g., M55A1 and SR19 as the first and second stages used in Minuteman missiles, Orion 50XL and

Orion 38 as the third and fourth stages taken from the Pegasus rocket. The hybrid rocket motors considered in the present analysis use cryogenic LOX, which requires low values of the mixture ratio to give high I_{sp} when burning with fuels containing hydrocarbons, and paraffin-based solid F as a propellant combination, which presents a good I_{sp}, a large regression rate coefficient (n), higher performance, and has a blowdown feed system [10]. The subsystems are updated in each iteration step based on the hybrid rocket propulsion characteristics and geometry, according to the optimization steps, leading to the attainment of the optimum solution. The literature gap in the launch vehicle design and optimization can be filled by modeling the interaction between aerodynamics, propulsion, structure, and trajectory subsystems in 6DOF simulation. Additionally, the performance of launch vehicles can be increased by using hybrid propulsion systems, which have lower production and manufacturing costs than other types of propulsion systems.

In the literature, there are articles in which simulations are conducted using 6DOF equations of motion. However, in recent literature studies involving optimization with the use of a 6DOF trajectory model, it is assumed that aerodynamic coefficients, center of gravity, and mass or moment of inertia values remain constant throughout the optimization process. In these studies, only simulation purposes are pursued without updating subsystems during optimization, and the focus is on finding the optimum values of a limited set of parameters [28–30]. On the other hand, while the research on hybrid rockets is expanding with an increasing number of publications, our study distinguishes itself by introducing a novel approach. In a pioneering contribution to the literature, our study introduces an optimization approach by using a 6DOF model that seamlessly integrates multiple subsystems, including aerodynamic, structural, environmental, propulsion, and trajectory components. This comprehensive integrated framework facilitates the interactive updating of subsystems throughout the optimization study for the first time in the literature. In our study, angular motion (three axes) and linear motion (three axes) are modeled as 6DOF. Throughout the optimization algorithm, it was observed that the location of the center of gravity, moments of inertia, and aerodynamic forces and moments change depending on the changing length of the launch vehicle after the separation of its stages. In our analysis, the effect of launch vehicle geometry was included in the study since the subsystems work interactively, and optimum results were obtained.

In other studies, only linear motion is considered since it is modeled as three degrees of freedom (3DOF), and only lift and drag are included in aerodynamics [31–35]. This aerodynamic lift and drag were extracted for the first geometry depending on the Mach number (M), that is, a new database was not created depending on the geometric change in aerodynamic forces. The 3DOF model stands out for its features of dynamic model simplification, saving on processor power and data processing capacity, and reducing system complexity. On the other hand, the importance of comprehensive modeling that is the closest representation to reality becomes evident in the optimization of subsystems with a dominant impact on the trajectory and performance of the launch vehicle, such as the propulsion system characteristics. However, in our study, we have the chance to examine the moment effects, namely the angular motion, together with other changes. As a different approach from other studies in the literature, an optimum result was successfully achieved while the effects that depend on geometrical changes in aerodynamic forces and the causes of these effects on the trajectory were observed.

In this respect, our study looks more comprehensively at the launch vehicle trajectory design problem and, for the first time, the effect of launch vehicle geometry works simultaneously with other parameters in the system, thanks to the interactive subsystems, and a successful optimum result was obtained. In our paper, Section 2 represents the modeling of hybrid launch vehicle subsystems, including aerodynamics, structural, and propulsion factors, as well as environment and gravity models. In Section 3, the main idea behind the optimization problem is defined in detail, along with the provided solution procedure. In Section 4, the comparison results with comprehensive modeling are evaluated. The discussions and conclusions are given in Section 5.

2. Modeling of Hybrid-Propellant Launch Vehicle

In this section, the subsystem models used in the optimization process are defined. The launch vehicle subsystems are coupled in a 6DOF simulation. Additionally, the current study attempts to fill the gap present in the literature for optimization that incorporates 6DOF integration and a model of subsystem couplings, including updates of subsystem parameters in each iteration during the optimization process. The proposed design and optimization study were applied to the Minotaur-I launch vehicle, and the results were obtained and evaluated. The Minotaur-I launch vehicle was chosen due to all its stages using a solid propellant. The Minotaur-I launch vehicle was also chosen due to the ease of modeling solid-propellant systems in simulation environments and the availability of reference mission data in the literature to compare with the optimization results. Minotaur-I, a member of the Minotaur rocket family produced by Orbital Sciences Corporation (now Northrop Grumman), is an American expendable launch system derived from the Minuteman II missile [36]. It is specifically designed for launching small satellites for the US Government. Minotaur-I stands at a height of 19.21 m and has a width of 1.67 m. Initially, launches of Minotaur-I were conducted from Space Launch Complex 8 at Vandenberg Air Force Base. The first successful flight carried The Joint Air Force-Weber State University Satellite (JAWSAT), an American military mini-satellite, on 27 January 2000, from Vandenberg Air Force Base. There has been a total of twelve successful launches of Minotaur-I. The launch vehicle consists of the M55A1 first stage and SR19 second stage, repurposed from a decommissioned Minuteman missile. Additionally, the third and fourth stages utilize components from the Pegasus rocket, specifically the Orion 50XL and Orion 38. Minotaur-I has proven its reliability, with the most recent launch being the NROL111 national security space payload for the National Reconnaissance Office, which took place on 15 June 2021, from NASA's Wallops Flight Facility.

2.1. Aerodynamic Model

Aerodynamic coefficients are critical parameters in the simulation model. These coefficients are utilized to understand the interaction and aerodynamic behavior of an object in the airflow. Used in simulation models, these coefficients play a crucial role in assessing and optimizing the performance of a launch vehicle. They assist engineers in improving their designs and optimizing aerodynamic performance. Therefore, aerodynamic coefficients have been incorporated into an aerodynamic model and integrated into the simulation tool. DATCOM, widely used semi-empirical aerodynamic prediction code, is utilized to calculate aerodynamic coefficients and integrate them into the flight mechanics subsystem [37]. DATCOM predicts aerodynamic forces, moments, and stability derivatives as a function of the α (angle of attack) and M (Mach number) for the desired flight condition based on the altitude and Reynolds number (Re). The static coefficients and dynamic derivatives of the aerodynamic coefficients are obtained as an output file. In-flight mechanics, the static coefficients, and the dynamic derivatives are combined to calculate aerodynamic forces and moments. This study considers drag, lift, and side forces, as well as rolling, pitching, and yawing moments. The aerodynamic coefficients are dependent on various parameters (precisely α, Re, and Mach); however, they are modeled to be dependent on three variables: α, sideslip angle (β), and M. The coefficients are obtained within the range of -20 to 20 degrees for α and β, and from 0 to 50 for M, ensuring they do not exceed the flight range. The study was conducted on a four-stage launch vehicle, and an optimization study was carried out by replacing the final stage with a hybrid-propellant motor. As the size of the final stage changes, the overall length of the launch vehicle is consequently altered. Therefore, adjusting the aerodynamic coefficients of the entire launch vehicle and each stage is necessary when each stage is separated. Aerodynamic coefficients are integrated into the simulation model and updated during the optimization process based on changes in the geometry of the launch vehicle. The geometry of the launch vehicle was modeled using MATLAB 2017b and integrated with the input file of the DATCOM program. Within this scope, during optimization, the stage length obtained from the propulsion model is used to update the DATCOM model through MATLAB 2017b, allowing the launch vehicle to be remodeled for the new geometry and obtaining updated aerodynamic coefficients without requiring additional inputs. Thus, by modeling the current state of the launch vehicle's aerodynamic performance and its effects on the flight, the challenge of treating them as constant values has been overcome.

2.2. Structural Model

Mass, moment of inertia, and center of gravity are fundamental parameters in flight simulation within the structural model. The mass value of the launch vehicle has a decisive impact on acceleration, velocity, and maneuverability. The moment of inertia determines the response to angular motions, influencing maneuverability. The center of gravity represents the balance point of the launch vehicle and affects stability if not in an appropriate position. Accurate modeling and simulation of these parameters are crucial to understanding how the launch vehicle will behave in real-world conditions. Careful tracking of these parameters in flight simulation is critical for safe and effective flight operations. In the design phase, accurately determining these parameters plays a significant role in optimizing the launch vehicle's performance and achieving the desired flight characteristics. Therefore, the vehicle structure serves as the mechanical interface between launch vehicles and all subsystems, making it crucial to obtain the most optimal design of the structural configuration to meet mission requirements. For the structural models of the Minotaur-I launch vehicle, CATIA V5R19 product design software was utilized [24]. The geometry, stage characteristics, and dimensions utilized in both the structural and aerodynamic models are depicted in Figure 1. It is important to highlight that the dimensions of the final stage were updated and optimized using a hybrid rocket motor and included in the optimization process.

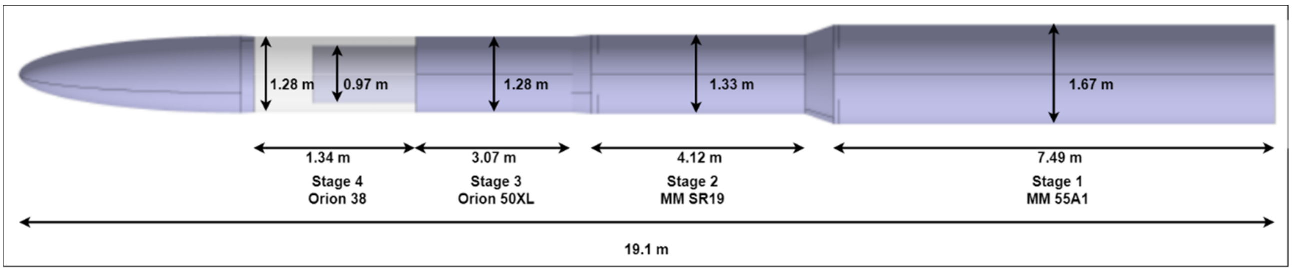

Figure 1. The representation of the Minotaur-I launch vehicle geometry used in structural and aerodynamic subsystems, obtained from DATCOM.

The case material of the first stage, MM 55A1, is D6AC steel, while the second stage, MM SR19, utilizes 6Al-4V titanium. The third stage, Orion 50XL, and the fourth stage, Orion 38, have monocoque graphite epoxy as their case material. Structural modeling was performed using the CATIA V5R19 CAD program [38]. Throughout the optimization, structural characteristics were updated by assuming the hybrid motor is made of 6Al-4V titanium also known as Grade 5 titanium, and mass and length calculations were performed in structural modeling. This material consists of 90% titanium, 6% aluminum, and 4% vanadium, offering an optimal combination of properties. With a density of 4430 kg/m^3 and a melting point around 1668 degrees Celsius, 6Al-4V titanium exhibits a tensile strength ranging from 900 to 1100 MPa, a yield strength typically between 800 and 1000 MPa, and an elastic modulus of approximately 114,000 MPa. Its hardness falls within the range of 36 to 44 HRC, while its fatigue strength is commendable [39]. The embedded presence of material properties within the CATIA V5R19 program facilitates the structural modeling. Its versatility allows for further processing to tailor it to specific applications [40]. The objective of this study was to comprehensively incorporate subsystem models into the optimization process, assuming the hybrid motor is made of 6Al-4V titanium, to iteratively update subsystems in each iteration cycle, aiming to obtain the most optimal design solution. In each iteration, due to changes in parameters such as geometry and mass values, aerodynamic coefficients, inertia moments, and center of gravity values are recalculated and updated. However, in this study, since the focus was on evaluating the performance and efficiency of the hybrid propulsion system and trajectory of the launch vehicle, and no research was conducted on structural concerns, structural aspects such as structural resistance, vibration, strength, and composition have not been investigated or analyzed. Therefore, structural calculations and modeling were performed at a fundamental level and incorporated into the optimization cycle.

For the first to third stages, the volumes of structural parts are determined based on known materials while the propellant volumes and heights are modeled using the propellant density (ρ_p) and structural part volume. However, the materials of the modified last stage (e.g., motor case, propellant, and oxidizer types) are currently unknown and assumed to be 6Al-4V titanium. The motor propellant parts and motor cases were modeled with the mentioned materials, ensuring a minimum distance of 2 cm between the motor case and the outer structural components. For example, as shown in Figure 1, the width of the fourth stage's motor case is 0.97 m, while that of the outer structural component measures 1.28 m. To obtain the mass (m) and inertia properties of the modified last stage, the CATIA V5R19 parametric design module was employed for modeling. During the optimization process, it is important to note that the structural and aerodynamic coefficients are updated based on the geometric changes obtained in each iteration to achieve results closer to reality by minimizing assumptions.

2.3. Environment Model

The environmental model is an indispensable element for enhancing flight safety, improving operational skills, and optimizing the design and performance of the launch vehicle. For this reason, the influence of the environmental effects on the performance and stability of air and space vehicles is also examined in our analysis. Various factors affect different types of vehicles but, for launch vehicles, the atmosphere and the Earth's gravity field are the dominant factors. Therefore, these two models are specifically considered in this study.

The gravity model plays a crucial role in flight simulation because flight involves understanding the movement of objects within the atmosphere based on these fundamental physical principles. During flight simulation, gravity constitutes the weight of the aircraft, and this weight is overcome by thrust to achieve the launch of the vehicle. *The EGM2008 gravity model* is a recent global high-degree potential model that offers significant advancements in obtaining precise trajectories for aerospace vehicles [41]. It simplifies the gravitational potential function to derive the gravitational acceleration function (GAF). The equation representing the GAF concerning Earth-centered Earth-fixed (ECEF) coordinates is given as Equation (1) [42]:

$$G_{J_2}^{ECEF} = -\frac{3}{2} J_2 \left(\frac{\mu}{r^2}\right) \left(\frac{a}{r}\right)^2 \begin{bmatrix} \left(1 - 5\left(\frac{z}{r}\right)^2\right) \frac{x}{r} \\ \left(1 - 5\left(\frac{z}{r}\right)^2\right) \frac{y}{r} \\ \left(1 - 5\left(\frac{z}{r}\right)^2\right) \frac{z}{r} \end{bmatrix} \tag{1}$$

where J_2 represents the zonal harmonic coefficient (1.08263×10^{-3}), μ represents Earth's gravitational constant (3.986×10^{14} m^3/s^2), r represents the distance of the launch vehicle from the center of mass of Earth, a represents the semi-major axis of Earth (6,378,137 m), and x, y, z represent the ECEF position of the launch vehicle.

The atmospheric model is used to predict the flight performance of launch vehicles and understand aerodynamic effects. The atmospheric model defines atmospheric parameters such as air density, pressure, and temperature based on the altitude of the launch vehicle. This information forms the basis for calculating significant forces in flight simulation, such as gravity, aerodynamic forces, and thrust. Consequently, flight simulations more accurately predict real flight conditions and play a crucial role in the design and optimization of launch vehicles. The *US1976 Standard Atmosphere Model (SAM)* was chosen for this study due to its combination of accuracy and simplicity [43]. This model provides the vertical distribution of atmospheric characteristics based solely on altitude (h). The outputs obtained from the US1976 SAM include temperature, pressure, speed of sound (T_{th}, P, Cs), and density (ρ). From these parameters, the M and dynamic pressure (P_{dyn}) can be derived. For $h > 84$ km, the atmospheric data are obtained analytically, where the tables are used for higher h [43]. The equations for $h > 84$ km and atmospheric data for higher h were implemented in the MATLAB environment using the research of NOAA, NASA, and USAF [43].

2.4. Propulsion Model

Playing a critical role in launch vehicle flight simulation, the propulsion model is a key determinant of the launch vehicle's thrust-generating capability and flight performance. This model encompasses the characteristics of the launch vehicle's motor, thrust, propellant consumption, and other parameters related to propulsion. In the simulation of a launch vehicle's flight, the propulsion model is utilized to calculate dynamic parameters such as the launch vehicle's velocity, altitude, and trajectory. Employed in optimizing the design of the launch vehicle, configuring the launch vehicle for a specific mission, and predicting the flight performance of the launch vehicle, this model holds significant importance. The accurate creation and integration of the propulsion model are crucial for ensuring the reliable and effective achievement of the launch vehicle's objectives. In this study, the effects and performance of fundamental characteristics of the propulsion system, such as thrust, total impulse, and specific impulse, were examined within the context of flight simulation. Effects related to combustion, internal ballistics, and similar factors within propulsion were not considered in this study. These effects have been addressed separately in dedicated studies outside the scope of flight simulation [44,45].

In the design and optimization problem, the hybrid propulsion equations, along with main T definitions and fundamentals, are utilized to calculate the propulsion characteristics of the modified last stage. The HTPB is chosen as the propellant due to its low cost, easy processing, and non-self-deflagration properties. The LOX, on the other hand, offers high safety and excellent performance at a low cost. The LOX/HTPB propellant combination is selected as it provides a non-toxic and relatively smoke-free exhaust while exhibiting similar chemical properties and performance to a LOX/kerosene bi-propellant system [46].

To determine the theoretical characteristic exhaust velocity (c^*) and specific heat ratio (k) for the reaction gases of the LOX/HTPB combination, a function of the mixture ratio is employed [46]. In the optimization study, the solution for the optimization problems incorporates a circular F grain port, as depicted in Figure 2. This choice is motivated by the ease of the production process and computational convenience. In the optimization process, the outside diameter of the modified vehicle is derived from the non-modified launch vehicle to prevent conflicts with the lower stages. The calculation of T coefficients is based on propulsion fundamentals [46].

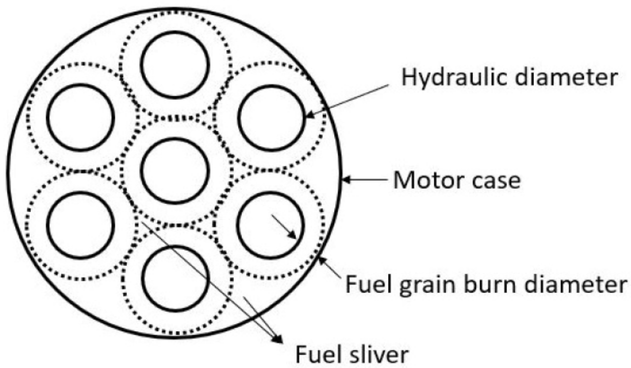

Figure 2. Circular fuel grain port.

The equation representing the combustion port radius (R) as a function of time (t) is provided as Equation (2) [46]:

$$R(t) = \left\{ a(2n+1)\left(\frac{\dot{m_O}}{\pi N}\right)^n t + R_i^{(2n+1)} \right\}^{1/(2n+1)} \quad (2)$$

where a, and n represent regression rate coefficients, $\dot{m_O}$ represents the mass flow rate of the oxidizer, and N represents the port number. For the chosen fuel combination of HTPB/LOX, empirical coefficients a and n, derived experimentally for specific propellant formulations, are 0.104 and 0.681, respectively. Additionally, the fuel grain port is set at 7.

Once R_i is determined, the F burn distance, oxidizer mass (m_O), initial F regression rate, and grain length are obtained using hybrid propulsion equations [46]. The total fuel mass, m_F, can be calculated using Equation (3):

$$m_F = \pi N \rho_F L \left[\left\{ a(2n+1)\left(\frac{\dot{m_O}}{\pi N}\right)^n t + R_i^{2n+1} \right\}^{\frac{2}{2n+1}} - R_i^2 \right] \quad (3)$$

where L represents the motor length and ρ_F represents fuel density. The thrust coefficient (C_F) is a valuable parameter in rocket propulsion as it allows for a normalized comparison of thrust performance across different systems, helping to assess efficiency and performance characteristics independent of specific engine size or operating conditions. C_F can be calculated using Equation (4) [46]:

$$C_F = \sqrt{\left(\frac{2k^2}{k-1}\left(\frac{2}{k+1}\right)^{\frac{k+1}{k-1}}\left(1-\left(\frac{p_2}{p_1}\right)^{\frac{k-1}{k}}\right)\right)} + \epsilon\frac{p_2}{p_1} \quad (4)$$

where p_1 represents chamber pressure and p_2 represents local pressure. C_F depends on the specific heat ratio k, the expansion ratio (ϵ), and the pressure ratio across the nozzle p_1/p_2, yet remains unaffected by chamber temperature. After calculating C_F, the thrust is determined using Equation (5) [46]:

$$F = C_F A_t p_1 \quad (5)$$

where A_t represents throat area, which is calculated from throat diameter, D_t ($A_t = \pi D_t^2/4$).

In the optimization process, m_O and total m_F are determined, and all propulsion parameters such as throat diameter, motor length, thrust, and specific impulse are updated based on the optimization design parameters to seek a feasible solution. During the propulsion characteristic calculations, it is assumed that the propulsion system operates with 95% efficiency. Furthermore, since the study was conducted in a vacuum region, it has been assumed that the thrust remains constant over time.

2.5. Trajectory Model

The trajectory model plays a crucial role in the simulation of launch vehicles as it encompasses all transformation functions between frames and translational and angular equations of motion. As it encompasses interactions between subsystems and serves as a bridge among them, it is essential to ensure the accuracy of the trajectory model to avoid irreversible situations. In this study, the 6DOF trajectory model was implemented using MATLAB 2017b in the optimization process [47]. The inclusion of the Coriolis term enables the calculation of angular velocities in the fixed-body coordinate system. The equation of angular motion is presented in Equation (6) [48]:

$$^{b}\dot{\omega}_{b/i}^{bf} = \left(J^{bf}\right)^{-1}\left[\mathbf{M}^{bf} - \omega_{b/i}^{bf} \times J^{bf}\omega_{b/i}^{bf}\right] \quad (6)$$

where $\omega_{b/i}$ represents the angular velocity of the body with respect to the inertial frame, $\dot{\omega_{b/i}}$ represents the time derivative of $\omega_{b/i}$, J represents the inertia matrix, and $\mathbf{M}$ represents the moment vector. J remains zero if the center of m of the body does not change during the motion. However, due to propellant consumption and stage separation, J changes during the flight. Therefore, J variations are also included in the model. To determine the state parameters of translational motion, Newton's second law of motion is applied. The position and velocity (V) of the launch vehicles are considered state parameters, considering the effects of propulsion, aerodynamics, atmosphere, and gravity. The equation for the translational acceleration vector of the body is given by Equation (7) [48]:

$$ {}^{e}\dot{\mathbf{v}}_{b/e} = \frac{1}{m}\mathbf{F} + \mathbf{G} - \omega_{e/i} \times (\omega_{e/i} \times \mathbf{P}_{cm/O}) - 2\omega_{e/i} \times \mathbf{v}_{b/e} \tag{7} $$

where $\mathbf{v}_{b/e}$ represents the velocity vector in the body frame with respect to ECEF, $\mathbf{F}$ represents the sum of the force vector, $\mathbf{G}$ represents the gravitation vector of Earth, $\mathbf{P}_{cm/O}$ represents the position vector of the body's center of mass in reference to the Earth's origin, and the e/i subscript represents ECEF concerning the inertial frame.

To solve the equations of motion, including centripetal and Coriolis accelerations due to the moving frame and rotating Earth, the fourth-order Runge–Kutta integration method is employed [49]. By solving the equations of motion, state parameters such as the position, velocity, angular orientation, and angular velocity of the launch vehicle are obtained, and the assessment is made as to whether it fulfills the objectives aimed at putting the payload into the targeted orbit.

3. Optimization of the Hybrid Last-Stage Launch Vehicle

Launch vehicle optimization is the process that enables the efficient and effective design and operation of launch vehicle systems used in space exploration and payload launches. It involves adjustments and improvements to ensure that the launch vehicle systems function in the most efficient manner possible during space research and payload launches. The main concept behind optimization problems is to determine optimization design parameters until the objective function reaches the desired minimum or maximum values. In the specific case of the hybrid last stage, the objective of the optimization is to determine the characteristics of the hybrid rocket motor such as throat diameter and certain flight path parameters, such as the TVC angle, to achieve a target trajectory for a specified PM.

The PSO algorithm was selected as the optimization method. The PSO algorithm falls under the category of swarm intelligence methods [50]. The use of SAs is motivated by their simplicity, robustness, and accuracy [51]. They are reported to be more efficient than GAs in terms of function evaluation and ease of implementation, while PSO is computationally more expensive compared to gradient-based methods [46,47]. However, there is a research gap in the application of PSO, particularly with a coupling strategy, in the field of hybrid small satellite launch vehicles. Therefore, the PSO algorithm is considered a promising and improvable optimization method.

PSO is a metaheuristic optimization algorithm inspired by the social behavior of birds and fish. In PSO, a population of potential solutions, called particles, moves through the solution space to find the optimal solution. Each particle represents a potential solution and is characterized by its position and velocity in the search space. The PSO algorithm operates through a dynamic iterative process. It begins with the initialization of a population of particles, each representing a potential solution to the optimization problem, and random assignments of positions and velocities. Parameters such as the number of particles, maximum iterations, and control factors are defined to guide the algorithm's behavior. In each iteration, the particles update their velocities based on a formula considering their past velocities, personal best positions, and the best position found by any particle in the swarm. These updated velocities are then used to adjust the particles' positions. The algorithm continually evaluates the fitness of these new positions, updating personal bests and the global best solution if improvements are found. The process iterates for a predefined number of iterations or until convergence is achieved, ultimately producing the best solution found as the output [23]. The hyperparameter settings for PSO include a swarm size of 100 particles to balance exploration and exploitation. The inertia weight starts around 0.9 and linearly decreases to 0.4 over iterations, regulating the balance between the particle's current and historical velocities. Acceleration coefficients are set to 2.0, controlling the influence of the particle's best known position and the global best known position on its movement.

The optimization problem for launch vehicles, specifically those with a modified last stage featuring hybrid propulsion, falls into the category of multi-objective design optimization. The subsystems within the launch vehicle are interrelated and exhibit coupling effects. For instance, the center of gravity location and inertia properties are calculated based on the new geometry obtained from CATIA, using the optimization design parameters. To ensure effective and realistic applications, the use of multi-objective multidisciplinary design optimization (MDO) algorithms is crucial for achieving more efficient and accurate optimization [52–54]. The flowchart outlining the multi-objective MDO approach and the interaction of the subsystems employed in this study for an example application of the Minotaur-I launch vehicle is depicted in Figure 3. This flowchart is not only applicable for the Minotaur-I launch vehicle but can also be utilized and generalized for other launch vehicles. In the flowchart, the optimization process begins with the determination of optimization design parameters to maximize the performance of the launch vehicle. This process starts with the identification of key elements, such as initial expansion ratio, initial chamber pressure, throat diameter, and thrust vector control of the first and last stages, which are optimization design parameters for the problem. Subsequently, the parameters relevant to these are calculated for the hybrid propulsion system. Then, the structural and aerodynamic features of the launch vehicle, whose geometric properties are computed, are calculated using software such as DATCOM Version 6 and CATIA V5R19. The trajectory of the launch vehicle is determined using calculated aerodynamic, structural, and propulsion subsystems along with environmental models such as gravity and atmosphere. Results obtained after each optimization step are stored, and an optimization algorithm is employed to optimize the performance of the launch vehicle. The obtained solution is determined through a fitness check to ascertain whether it meets design constraints such as targeted orbit parameters. If not, the optimization design parameters are adjusted, and the optimization process is iterated. Ultimately, upon completion of this comprehensive process, the launch performance of the launch vehicle is successfully optimized.

For the optimization study, the Minotaur-I launch vehicle was selected to determine the hybrid propulsion characteristics and TVC angle required to achieve the desired trajectory. This launch vehicle consists of four solid stages. Detailed information regarding the launch vehicle, including its geometry, stage masses, and structural and propulsion characteristics, can be found in Figure 1 and Table 2 [55]. The first stage is 7.49 m in length, with a diameter of 1.67 m and a mass of 23,077 kg. This stage has a thrust power of 792 kN in a vacuum, and the burn time of its motor is 61.3 s. The second stage, with a shorter length of 4.12 m, a diameter of 1.33 m, and a mass of 7032 kg, is equipped with a motor that produces 267.7 kN of thrust, and its burn time is 66 s. The third stage measures 3.07 m in length and 1.28 m in diameter, with a mass of 4036 kg. With a thrust of 194.4 kN, this stage has a motor burn time of 71 s. The final stage is 1.34 m in length, has a diameter of 0.97 m, and a mass of 872.3 kg. Its motor produces a thrust of 36.9 kN, and the burn time is 66.8 s.

The optimization process focuses on modifying the last stage of the Minotaur-I launch vehicle by incorporating a hybrid propulsion system. This modification aims to improve performance and achieve an efficient design. The target mission requires orbit parameters of h = 741.2 km and related inclination for target orbit altitude, i = 98.3°, for a sun-synchronous orbit (SSO), with a PM of 302 kg [56]. During the optimization process, the input parameters are adjusted within the defined limits of the design space.

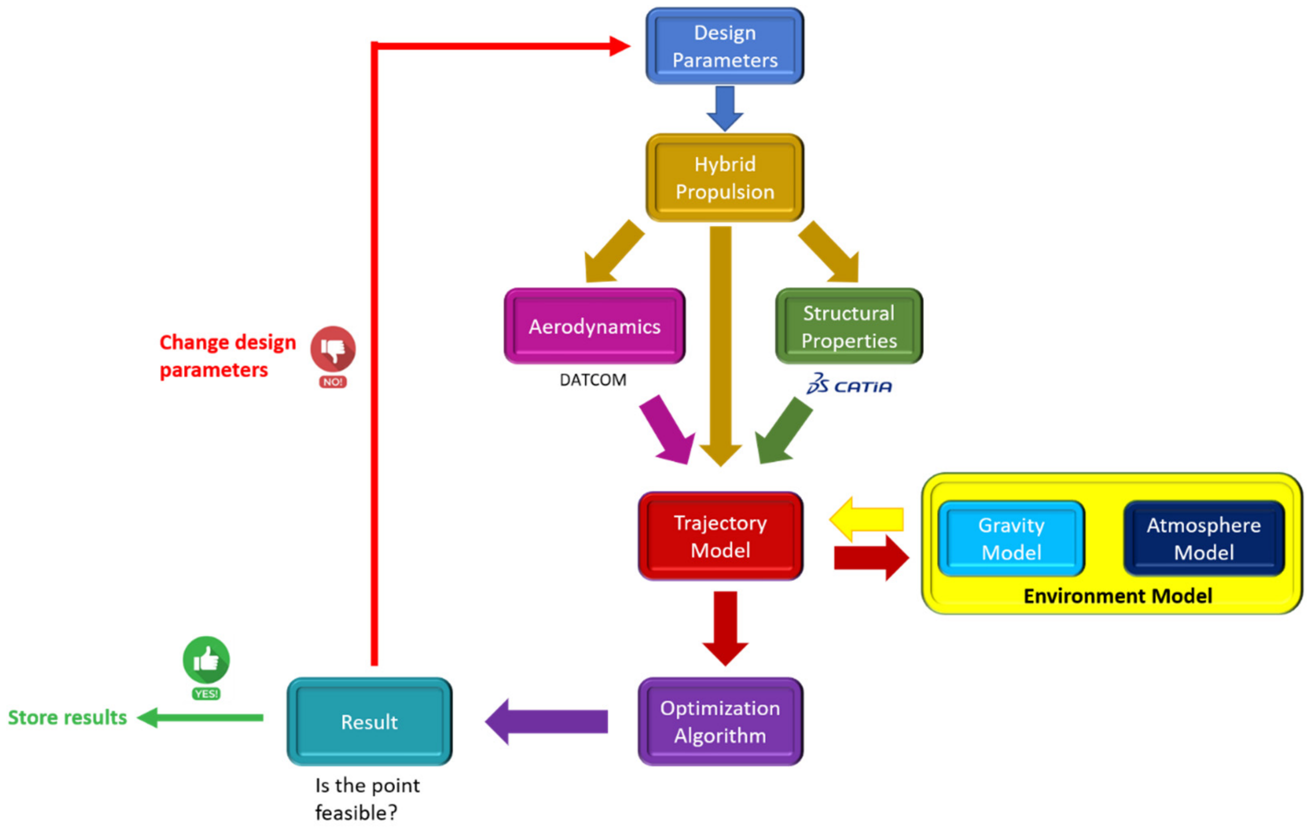

Figure 3. Flowchart of coupled analysis and multi-objective MDO approach.

Table 2. Minotaur-I launch vehicle characteristics.

	Stage 1	Stage 2	Stage 3	Stage 4
L, m	7.49	4.12	3.07	1.34
D, m	1.67	1.33	1.28	0.97
m_g, kg	23,077	7032	4036	872.3
T, kN (Vacuum)	792	267.7	194.4	36.9
t_{burn}, s	61.3	66	71	66.8

Mathematically, the optimization problem can be defined as shown in Equation (8). The objective is to determine the optimal values for the propulsion characteristics of the hybrid stage and the TVC angles of the first and last stages. These values should maximize the total impulse-to-weight ratio (I_t/w_0) while adhering to I_{sp} constraints and ensuring the target orbit parameters are met, as stated in Equations (9)–(12). The objectives are:

$$\max_{\forall s \in \mathbb{R}} I_t/w_0(s) \text{ and } \min_{\forall s \in \mathbb{R}} \Delta\gamma(s), \Delta h(s), \Delta V(s) \tag{8}$$

To maintain consistent consideration of objectives throughout the optimization process, the percentage errors in target orbit parameters, specifically flight path angle, altitude, velocity (γ, h, V), and ($1/(I_t/w_0)$), are scaled by a factor of 10 to align the magnitudes of these errors. For example, in this study, the value of ($1/(I_t/w_0)$) is of an order of magnitude approximately 1/10 lower than the other objectives. Therefore, the value of ($1/(I_t/w_0)$) is multiplied by 10 in the optimization process to bring all objectives to the same order of magnitude and to achieve the most optimal solution [57]. This incorporation of scaled terms enables comparable effects of the objectives in the optimization process. The objectives are subjected to the following constraints and the subscript t denotes target parameters:

$$g_1(s) = 1 - \frac{I_{sp}(s)}{287\ s} \leq 0 \ \ g_1(s)\epsilon\mathbb{R} \tag{9}$$

$$g_2(s) = \frac{h - h_t}{h} \times 100 - 1 \leq 0 \ \ g_2(s)\epsilon\mathbb{R} \tag{10}$$

$$g_3(s) = \frac{V - V_t}{V} \times 100 - 1 \leq 0 \ \ g_3(s)\epsilon\mathbb{R} \tag{11}$$

$$g_4(s) = \frac{\|\gamma\|}{0.2\mathrm{deg}} - 1 \leq \ 0\ g_4(s)\epsilon\mathbb{R} \tag{12}$$

The specific impulse of the Minotaur-I launch vehicle's solid last-stage motor is 287 s, and it can tolerate a flight path angle of 0.2 degrees [56]. Therefore, these values were entered into the objective equations. The optimization parameters, represented as design variables, are continuous parameters that span between the lower limit $\mathrm{s_L}$ and upper limit $\mathrm{s_U}$. The range of these optimization parameters is defined as $\mathrm{s_L} \leq \mathrm{s} \leq \mathrm{s_U}$. The specific optimization parameters can be seen in Equation (13):

$$\mathrm{s} = \{\mathrm{TVC_{first}},\ \mathrm{TVC_{last}},\ \mathrm{t_{burn}},\ p_1,\ \mathbf{MR},\ \epsilon,\ \mathrm{D_t}\} \tag{13}$$

where **MR** represents the initial mass ratio, $\mathrm{t_{burn}}$ represents burn time, $\mathrm{D_t}$ represents throat diameter, p_1 represents the initial chamber pressure, ϵ represents the initial expansion ratio, and $\mathrm{TVC_{first}}$ and $\mathrm{TVC_{last}}$ represent the TVC angle of the first and last stage, respectively. The optimization design parameter primarily contributes to process and performance enhancement, while the launch vehicle design parameter plays a role in determining the physical structure and functionality. The optimization design parameters can play a dual role, serving as inputs both in the propulsion system and along the trajectory calculations, providing information about the launch vehicle's performance and efficiency. The optimization parameters were assigned lower and upper limits as follows: $0 \leq \mathrm{TVC_{first}} \leq 6°$, $1 \leq \mathrm{TVC_{last}} \leq 3°$, $20 \leq \mathrm{t_{burn}} \leq 60$ s, $2 \leq p_1 \leq 4$ MPa, $1 \leq \mathbf{MR} \leq 3$, $7.5 \leq \epsilon \leq 11$, and $0.065 \leq \mathrm{D_t} \leq 0.15$ m. The lower and upper limits were chosen to ensure physical feasibility. The trajectory properties of h, V, and γ serve as both objective and constraint parameters to optimize the operation effectively and efficiently. When objectives are also entered as constraints, especially because the targeted orbit parameters need to be met, it guides the algorithm to find solutions closest to these parameters. The optimization process aims to minimize or maximize the objective functions while satisfying the constraints and requirements to obtain a feasible solution. For this study, the modeFRONTIER 2019R1 optimization software is utilized as a multidisciplinary optimization solver, equipped with an automatic framework [57]. The flow scheme of the multi-objective multidisciplinary optimization process, along with the steps involved in solving the optimization problem, is illustrated in Figure 4. In Figure 4, $\mathrm{t_{burn}}$, p_1, $\mathrm{TVC_{first}}$, $\mathrm{TVC_{last}}$, **MR**, $\mathrm{D_t}$, and epsilon in the design parameters represent $\mathrm{t_{burn}}$, p_1, $\mathrm{TVC_{first}}$, $\mathrm{TVC_{last}}$, **MR**, $\mathrm{D_t}$, and ϵ, respectively. The process begins with "SchedulingStart", indicating the initiation of the optimization routine using multi-objective particle swarm optimization (MOPSO), a technique for solving problems with multiple objectives. Under the heading "Design Parameters", a compilation of variables amenable to modification during optimization is presented, encompassing parameters such as burn time, chamber pressure, TVC angle of the first and last stages, mass ratio, throat diameter, and expansion ratio. These parameters serve as inputs to the optimization process and are subject to iterative adjustments aimed at identifying the optimal solution. The workflow then moves to a script, suggesting a computational step, to calculate initial values and prepare data for optimization. At this stage, MATLAB scripts are employed, primarily for computations related to hybrid characteristics utilizing the optimization design parameters, thus aligning with the overarching objectives and constraints. The calculation steps involved in this study cover various aspects, including hybrid rocket propulsion, CATIA-based structural properties such as mass and inertia characteristics, aerodynamic characteristics, and trajectory determination, which are systematically executed. The initial phase of the optimization process involves the calculation of hybrid rocket propulsion characteristics. Subsequently, the obtained motor length and hybrid stage mass serve as inputs for the structural model, created using parametric shape design in the CATIA program. In this stage, the values for the center of gravity and moment of inertia, which vary as stages are ejected and propellant is consumed, are determined for the entire launch vehicle and its stages. All the pertinent information is then iteratively integrated into the flight mechanics 6DOF model within the optimization main file until feasible solutions are achieved, satisfying the specified constraints and objectives. Within the 6DOF simulation, the subsystems of aerodynamics, propulsion, structure, and trajectory are intricately interconnected. This interdependence signifies that the outputs produced by the propulsion subsystem serve as inputs for both the trajectory and structural subsystems. Downstream from the MATLAB step, the workflow branches into objectives and constraints. The objectives prefixed with "Objective", such as "Objective_fpa", "Objective_h", and "Objective_V", represent the desired outcomes for the flight path angle, altitude, and velocity, respectively. The constraints prefixed with "Constraint_", such as "Constraint_fpa", "Constraint_h", and "Constraint_V", denote the limits and requirements that the optimization process must not break for the flight path angle, altitude, and velocity. The process concludes with an "Exit" node, signaling the end of the optimization routine, after which the best solution or set of solutions may be selected based on the objectives and constraints defined. This flowchart provides a structured representation of the optimization process, highlighting the parameters involved, the computational tools employed, and the performance metrics that guide the search for an optimal design and trajectory of the launch vehicle.

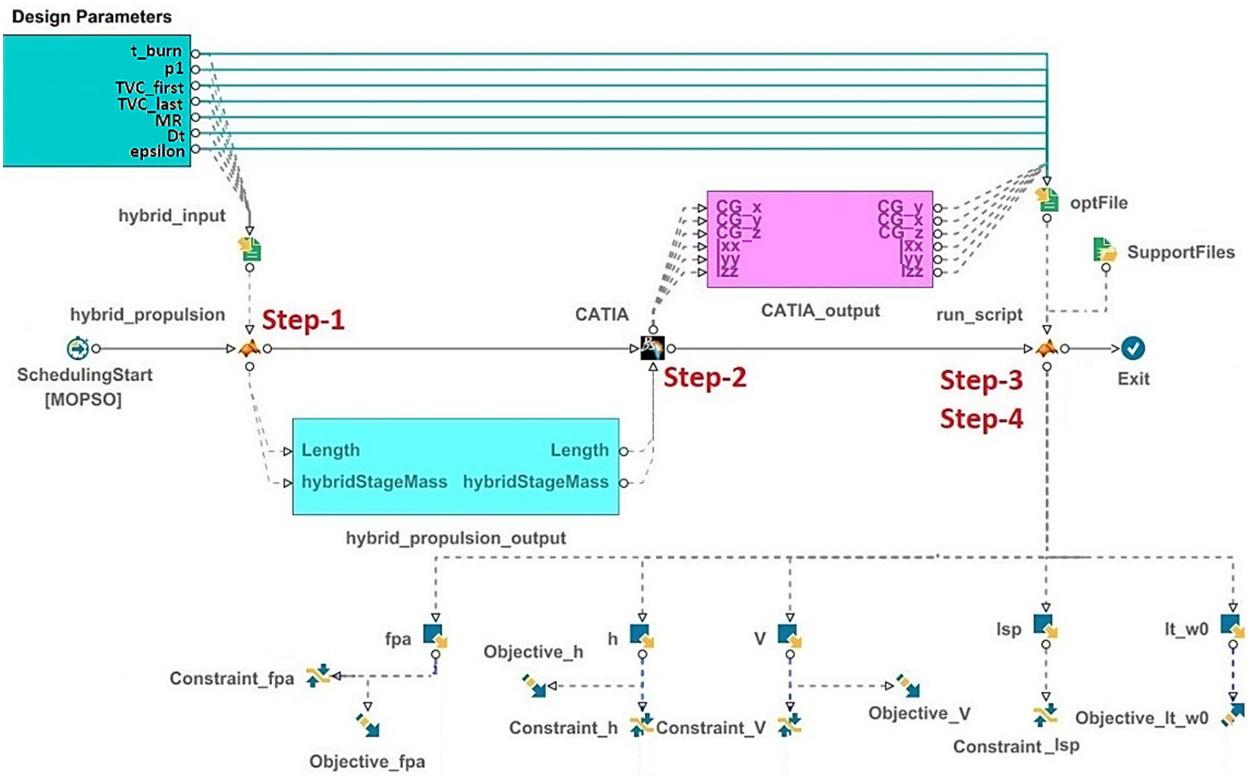

Figure 4. Workflow of the multi-objective multidisciplinary optimization process.

The calculation steps involve hybrid propulsion, CATIA-based structural properties, aerodynamics characteristics, and trajectory determination. In the 6DOF simulation, the aerodynamics, propulsion, structure, and trajectory subsystems are coupled. This coupling implies that the outputs of the propulsion subsystem serve as inputs to the trajectory and structural subsystems, and vice versa. The specific couplings between subsystems are defined in Table 3. The table encompasses the input and output parameters among the subsystems of the launch vehicle. The columns indicate whether each parameter serves as an input for a given subsystem, while the rows specify whether the parameters act as outputs from the subsystems. From the propulsion subsystem, information such as thrust and propellant mass is provided to the trajectory model; stage length, propellant mass, and stage diameter are provided to the structural model; and motor length and motor diameter are provided to the aerodynamic model. The structural subsystem supplies center of gravity and moment of inertia information to the trajectory model and center of gravity information to the aerodynamic model. From the aerodynamics model, aerodynamic coefficient details are provided for the trajectory model. Conversely, the trajectory model supplies Mach number, angle of attack, and sideslip angle information to the aerodynamic model.

Table 3. The couplings between subsystems of launch vehicles.

Subsystems	Trajectory	Structure	Aerodynamics
Propulsion	thrust propellant mass	length propellant mass diameter	length diameter
Structure	center of gravity moment of inertia	-	center of gravity
Aerodynamics	-	-	Mach number angle of attack side slip angle

The optimization process was executed on a workstation equipped with an Intel Xeon Silver 4216 CPU operating at 2.10 GHz, 64 cores, and 128 GB RAM. The process runs for approximately 8 h and 11 min. To expedite the process, 30 models were created and run simultaneously in parallel. The initial design parameters were selected using the design of the experiment methodology. Throughout the optimization process, the design parameters were constrained to scan a wide range. However, due to the simultaneous fulfillment of targeted trajectory parameters being a highly challenging criterion, it has been observed that as the iteration steps progress during optimization, the algorithm converges until the global optimum solution is reached, and the optimization process is terminated. A total of 30,000 iterations were performed, resulting in 29,688 unfeasible designs and 310 errors. An unfeasible solution indicates that a specific point in the design space cannot be physically realized. In other words, it denotes situations where constraints related to that design configuration are not satisfied or conflict. Errors signify a potential issue with simulation or analysis tools. This could be due to various reasons such as an error in input parameters, model configuration, or missing/corrupted data files. However, since only 1.03% of the entire solution space is affected, it does not carry critical importance in the optimization solution here. Moreover, two feasible points were obtained for the multi-objective multi-disciplinary problem. The reasons for finding a few feasible points lie in the complexity of multi-stage launch vehicles and hybrid-propellant motor optimizations. Additionally, the scarcity of feasible points indicates that solutions meeting specific constraints, such as providing required orbit parameters for placing the payload into the targeted orbit, may be limited. The constraints narrow down the solution space, reducing the number of viable points. In these optimization problems, it is crucial to ensure the physical feasibility of the found solutions, achieve practical optimal results, and performance improvement [58,59].

Upon successful completion of the optimization process, feasible designs and the corresponding broken constraints are acquired. These results are presented in Figure 5, where each bubble with a red foreground marker represents a feasible solution. Due to the complexity of the multi-objective multidisciplinary problem, the plot specifically showcases the minimum flight path and minimum V error constraints. Furthermore, Table 4 provides the properties of the feasible points displayed in Figure 5. The broken constraint pie chart illustrates the percentage values at which constraints are broken for all design points obtained throughout the entire optimization process. This enables an assessment of which constraint is more challenging.

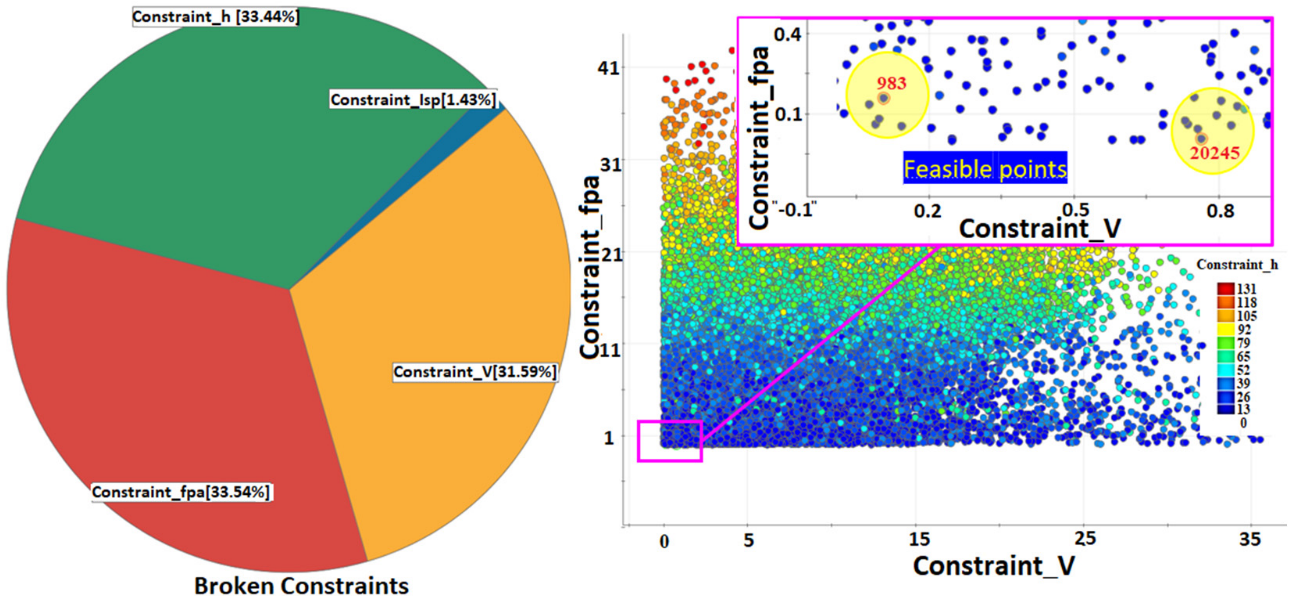

Figure 5. Broken constraints and distribution of the feasible designs for γ, h, V.

Table 4. The properties of feasible solutions.

Design ID	D_t, m	TVC_1, deg	t_b, s	p_2, MPa	ϵ	MR
983	0.085	4.824	34.71	3.709	9.15	1.945
20245	0.095	4.882	36.65	2.678	8.55	2.765
Design ID	**TVC_4, deg**	**I_{sp}, s**	**V, m/s**	**γ, deg**	**h, km**	
983	2.062	313.88	7474.2	−0.159	738.2	
20245	1.729	308.95	7425.1	−0.007	747.6	

Observing the broken constraints in Figure 5, it can be noted that the γ, h, and V constraints are broken to a similar extent in the broken constraint percentages, while the I_{sp} constraints exhibit smaller deviations compared to other constraints. In this problem, it is indicated that all constraints, namely γ, h, and V, are equally important for achieving the required orbital parameters to place the payload into the targeted orbit. If any of these constraints are not met, the payload cannot be placed into the targeted orbit. This highlights the challenge of simultaneously satisfying all these constraints. On the other hand, aiming for a higher specific impulse than the solid-propelled original stage (287 s) is less restrictive relative to other constraints, and limits on design points with lower specific impulse have been broken. Therefore, while it can be stated that performance improvement is achieved with an I_{sp} value greater than 287 s, it can be explicitly expressed that the mission is unsuccessful when any of the orbital parameters cannot be fulfilled. As a result, a few feasible points are obtained in the optimization solution. A Pareto optimal point represents a solution in multi-objective optimization where no further improvement in one objective can occur without compromising another. This concept enables decision-makers to explore trade-offs and identify balanced solutions that maximize multiple objectives simultaneously, offering a comprehensive and efficient approach to complex optimization problems. As Design ID 20245 points to a Pareto optimal solution, the results of Design ID

20245 in this study were compared with the original Minotaur-I launch vehicle. Figure 6 provides the comparison of trajectory, velocity, and flight path during the flight for the optimization results of Design ID 20245 for the hybrid last stage, along with the reference points of the solid last stage, for the Minotaur-I launch vehicle [56].

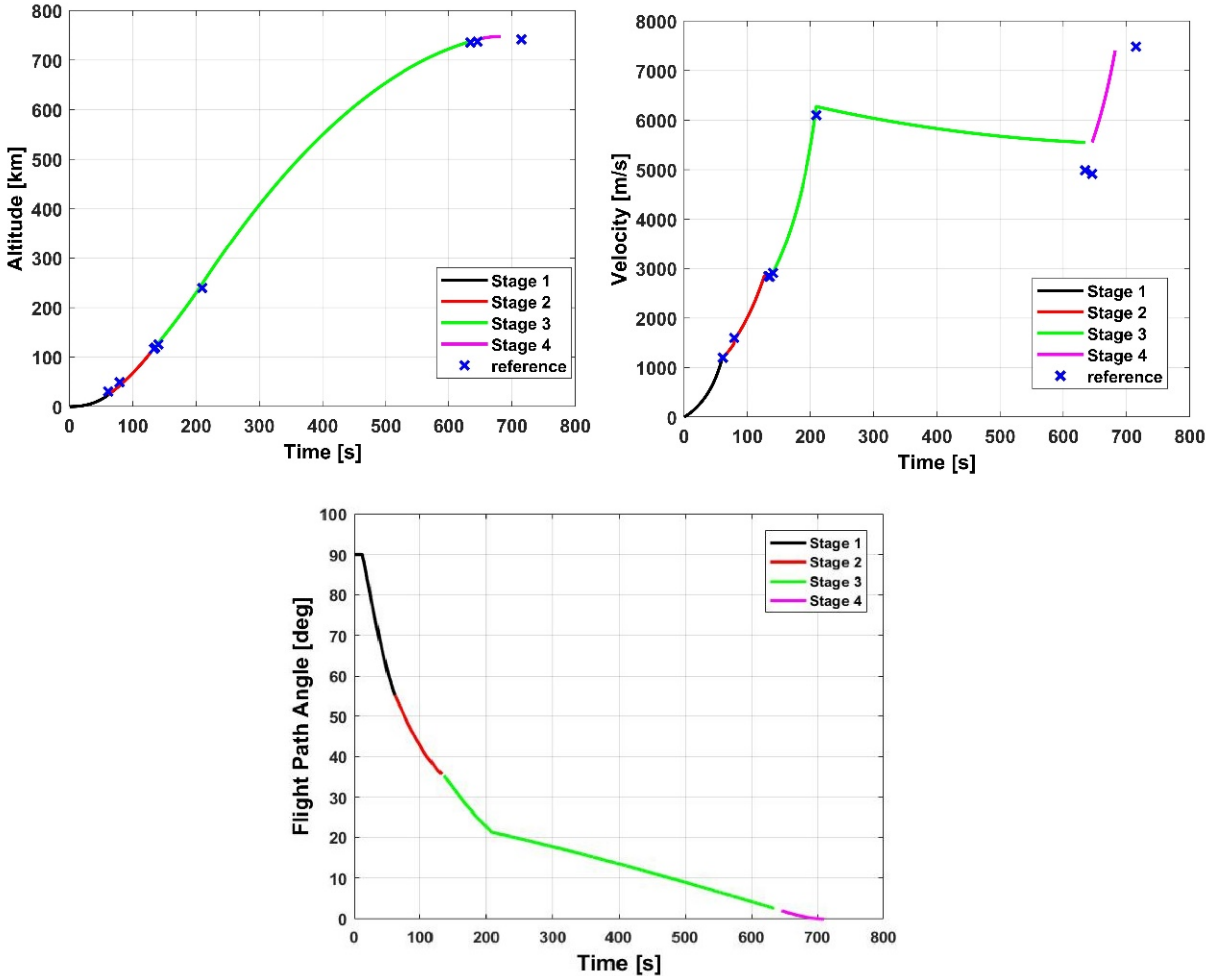

Figure 6. The trajectory of Design ID 20245 and reference points.

When Figure 6 is examined, it is observed that the values obtained because of the optimization study led to reaching the target orbit in a shorter time than the reference, and in the cruise flight phase, the final stage experiences less speed loss due to being lighter than the reference. The flight path angle gradually decreases and approaches zero after the steep climb, as expected.

Tables 5 and 6 provide a comparison between the trajectory and propulsion characteristics of Design ID 20245 and the reference values. It is noted that the altitude reached as a result of the optimization is 747.6 km, which is 0.863% different from the target orbit altitude of 741.2 km. Furthermore, the velocity required for the payload to reach the target orbit is 7482.2 m/s. The velocity achieved as a result of optimization is 7425 m/s, with a 0.763% difference from the reference value. The change in propellant type, transitioning from HTPB to HTPB/LOX, indicates the use of an oxygen-enhanced hybrid propulsion system. This alteration is particularly noteworthy in the m_p parameter; while Minotaur-I has a mass of 770.2 kg, this value has decreased to 416.2 kg in the optimized Minotaur-I-like configuration. Additionally, significant differences are observed in the stage length and thrust values. In the optimized configuration, Minotaur-I-like has increased the L^* value from 1.34 m to 2.93 m, but this has led to a decrease in T (from 36.9 kN to 34.48 kN). As a result of these changes, the I_{sp} value has substantially increased from 287 s to 308.95 s, indicating that the rocket operates more efficiently. Moreover, t_{burn} has significantly decreased in the Minotaur-I-like configuration, going from 66.8 s to 36.65 s. This implies that the rocket can complete its mission in a shorter time frame. Finally, I_t/w_0 has increased in the Minotaur-I-like configuration, from 253.3 to 257.7. This signifies that the launch vehicle, relative to its total mass, provides more thrust, optimizing its performance. These changes demonstrate that Minotaur-I-like, compared to the Minotaur-I configuration, is an optimized design that achieves significant improvements in specific performance metrics.

Table 5. Trajectory comparison of optimization results and reference points.

Parameters	Target	Optimization Results	Absolute Error
h, km	741.2	747.6	0.863%
V, m/s	7482.2	7425	0.763%
γ, deg	0	−0.00742	-

Table 6. Propulsion comparison of optimization results and reference points.

Parameters	Minotaur-I	Minotaur-I-Like (Hybrid)
Propellant type	HTPB	HTPB/LOX
m_p, kg	770.2	416.2
L^*, m	1.34	2.93
T, kN	36.9	34.48
I_{sp}, s	287	308.95
t_{burn}, s	66.8	36.65
I_t/w_0	253.3	257.7

4. Comparison of the Comprehensive Modeling

This study was compared with 3DOF, aiming to identify the advantages and differences arising from comprehensive modeling in optimization problems. In this context, 3DOF model outputs were obtained for both the hybrid last-stage launch vehicle and the original Minotaur-I launch vehicle using 6DOF inputs. Furthermore, the differences due to detailed subsystem modeling were also highlighted.

The percentage differences in altitude, velocity and flight path angle in flight mechanics when using a 6DOF model are generally smaller compared to those using 3DOF, especially for complex maneuvers and simulations that involve precise positioning and interactions with the environment [44]. For advanced flight simulations, such as those used in aerospace engineering, a 6DOF model is preferred because it can provide highly accurate results, often within a few percentage points of reality. For example, Brochu and Lestage indicate that the relative error between the 3DOF and 6DOF models for maximum range envelope calculations is 3% and 12% at altitudes of 1 and 15 km, respectively [60]. Therefore, as the flight simulation time increases, the difference between 3DOF and 6DOF models will gradually become more pronounced. To demonstrate the accuracy of the results, we compare the 3DOF and 6DOF simulations obtained for the same design point, Design ID 20245, and the original Minotaur-I launch vehicle, and discuss the differences between these simulations. A comparison is made with the results of Design ID 20245, as it provided results quite close to the reference values given for the trajectory of the original Minotaur-I launch vehicle, and this study aims to examine the difference between the 3DOF outputs and those of 6DOF. The altitude and velocity graphs obtained over time from the 3DOF and 6DOF simulations are presented for the hybrid last stage as the output of the optimization process in Figure 7, and for the original solid last stage that is taken as the reference data of the Minotaur-I launch vehicle in Figure 8, and the percentage differences $\left(\left|\frac{\text{value}-\text{targetvalue}}{\text{targetvalue}}\right| \times 100\right)$ between the target altitude and velocity are given in Tables 7 and 8, respectively.

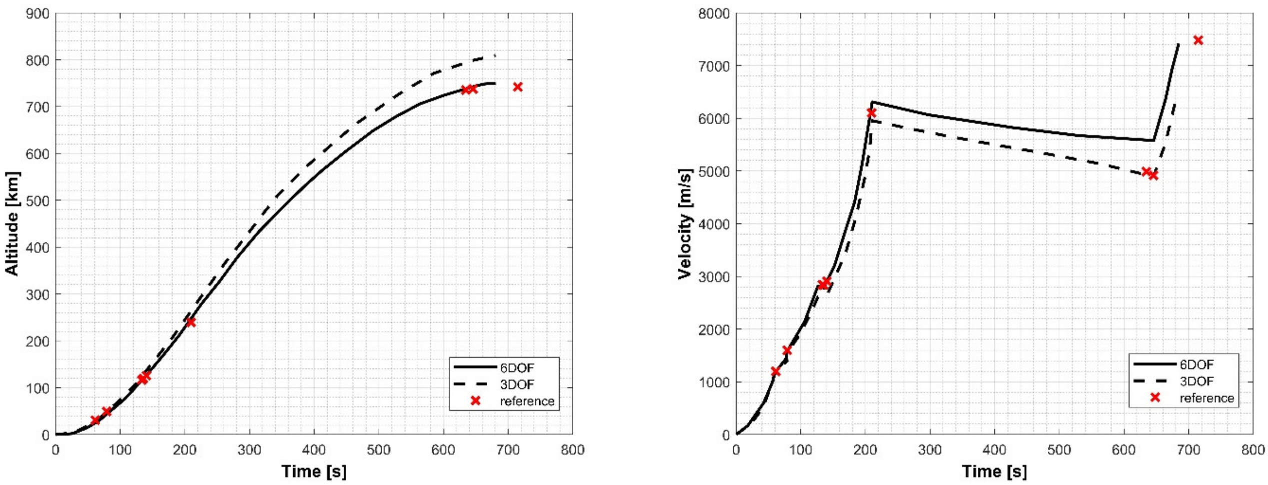

Figure 7. The simulation results of the 3DOF model and 6DOF model for the hybrid last stage.

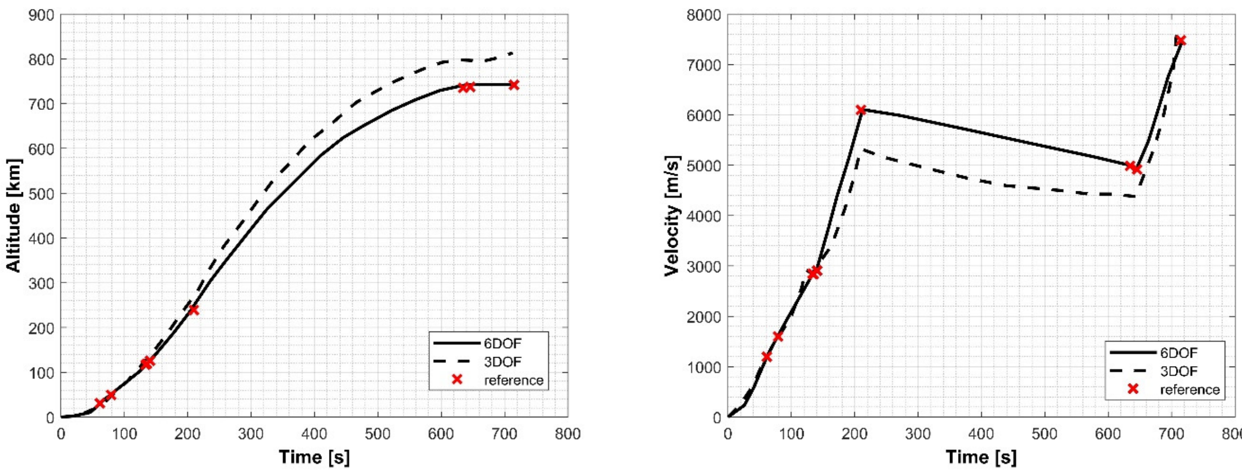

Figure 8. The simulation results of the 3DOF model and 6DOF model for the original Minotaur-I launch vehicle.

Table 7. The comparison summary of 3DOF and 6DOF results for the hybrid last stage.

	6DOF	**3DOF**	**Target**	**% Difference (6DOF/3DOF)**
V, m/s	7425	6567	7482.2	0.76/11.55
γ, deg	−0.0074	7.2708	0	-
h, km	747.6	807.6	741.2	0.86/8.02

Table 8. The comparison summary of 3DOF and 6DOF results for the solid last stage.

	6DOF	**3DOF**	**Target**	**% Difference (6DOF/3DOF)**
V, m/s	7460.2	7587.4	7482.2	0.29/1.41
γ, deg	0.0052	2.665	0	-
h, km	743.7	812.4	741.2	0.34/9.61

As seen from Figures 7 and 8, it can be observed that the difference between the 3DOF and 6DOF simulations widens as flight time progresses. Therefore, since the values obtained from the 6DOF simulation, especially for the original Minotaur-I launch vehicle, align with the reference, it can be said that, especially for long-duration missions, the accuracy of the results obtained from the 6DOF simulation is higher compared to that from the 3DOF simulation. Due to the reasons highlighted in Tables 5 and 6, while the final values obtained through optimization for Design ID 20245 appear similar to the reference values, slight differences are observed at lower stages. Meanwhile, it is observed that the difference between the results of 3DOF and 6DOF models is gradually widening. Additionally, it is noticed that the deviation rate of the results obtained with 3DOF from the target values is also higher.

When Table 7 is examined, in the 3DOF model, complex angular velocity calculations, such as those found in the 6DOF model, are not present. Additionally, effects like moment of inertia, center of mass, and moment changes are not included, causing the gap between the two models to widen as the simulation progresses. Firstly, when we examine the velocity (V) parameter, it is observed that the 6DOF model reaches a speed of 7425 m/s, while the 3DOF model reaches 6567 m/s. The target speed is set at 7482.2 m/s, and in this case, it is observed that the 6DOF model deviates by 0.76%, whereas the 3DOF model deviates by 11.55%. Focusing on another parameter, the flight path angle (γ), the 6DOF model achieves -0.0074 degrees, while the 3DOF model reaches 7.2708 degrees. The target angle of attack is set at 0 degrees, and in this situation, it is observed that the 6DOF model is closer to this target, whereas the 3DOF model exhibits a significant deviation. Lastly, when we concentrate on the altitude (h) parameter, the 6DOF model reaches an altitude of 747.6 km, while the 3DOF model reaches 807.6 km. The target altitude value is set at 741.2 km, and in this case, it is observed that the 6DOF model deviates by 0.86%, whereas the 3DOF model deviates by 8.02%. This analysis provides a detailed insight into the performance differences between the two models.

According to Table 8, examining the velocity parameter, we observe that the 6DOF model achieves a velocity of 7460.2 m/s, while the 3DOF model reaches 7587.4 m/s. The target V is set at 7482.2 m/s. In this context, the 6DOF model exhibits a slight deviation of 0.29%, while the 3DOF model shows a slightly higher deviation of 1.41%. Shifting the focus to γ, we find that the 6DOF model attains a value of 0.0052 degrees, whereas the 3DOF model reaches 2.665 degrees. The target flight path angle is specified as 0 degrees. Remarkably, the 6DOF model aligns closely with this target, demonstrating negligible deviation, while the 3DOF model shows a notable deviation of 2.665 degrees. Considering the h parameter, the 6DOF model reaches an altitude of 743.7 km, while the 3DOF model achieves 812.4 km. The target altitude is set at 741.2 km. Consequently, the 6DOF model displays a modest deviation of 0.34%, while the 3DOF model exhibits a more substantial deviation of 9.61%. While the 6DOF model closely aligns with the targeted parameters, it is evident that the 3DOF model results obtained by running with the parameters entered into the 6DOF model deviate from the targeted parameters. Therefore, it can be concluded that more detailed models like the 6DOF model provide more accurate results, while 3DOF models are more suitable for rapid calculations where precise results are not expected. It can be observed that using 6DOF models, especially in critical tasks during the design phase, can lead to obtaining more precise results, particularly in satellite launch vehicle projects that require high precision. This, in turn, could potentially shorten the design process, and comprehensive modeling with 6DOF solutions can yield results closer to reality.

In order to elaborate on comprehensive modeling and to observe the difference resulting from comprehensive modeling, 6DOF results were obtained without a change in the center of gravity, without considering the change in moment of inertia, with constant aerodynamic coefficients, and by combining three scenarios, i.e., without comprehensive modeling. The comparison summaries of comprehensive modeling for the hybrid last stage and solid last stage are presented in Tables 9 and 10, respectively.

Table 9. The comparison summary of comprehensive modeling results for the hybrid last-stage vehicle.

			Without CG Change		Without Inertia Change	
	6DOF	**Target**	**Results**	**% Difference**	**Results**	**% Difference**
V, m/s	7425	7482.2	6603.8	11.06	6499.4	12.47
γ, deg	−0.0074	0	21.8	-	−8.54	-
h, km	747.6	741.2	1249.4	68.6	896.02	20.9
			Constant Aero		**Combined 3 Cases**	
	6DOF	**Target**	**Results**	**% Difference**	**Results**	**% Difference**
V, m/s	7425	7482.2	6195.5	16.56	4613.5	37.87
γ, deg	−0.0074	0	27.41	-	80.03	-
h, km	747.6	741.2	1546.61	108.7	2417.6	226.2

Table 10. The comparison summary of comprehensive modeling results for the original Minotaur-I launch vehicle.

			Without CG Change		Without Inertia Change	
	6DOF	**Target**	**Results**	**% Difference**	**Results**	**% Difference**
V, m/s	7460.2	7482.2	6690.4	10.6	6301.3	15.8
γ, deg	0.0052	0	16.5	-	−6.9	-
h, km	743.7	741.2	1102.6	48.8	913.4	23.2
			Constant Aero		**Combined 3 Cases**	
	6DOF	**Target**	**Results**	**% Difference**	**Results**	**% Difference**
V, m/s	7460.2	7482.2	6023.4	19.5	4209.2	43.7
γ, deg	0.0052	0	31.8	-	77.1	-
h, km	743.7	741.2	1325.9	78.9	2269.3	206.2

Table 9 provides a comprehensive comparison of modeling results for the hybrid last stage, considering different scenarios involving variations in center of gravity, moment of inertia, and constant aerodynamics. The table includes results for the 6DOF model, comparing them to the target values, and showcases the percentage differences for each specific case. Looking at the V parameter, the 6DOF model's initial result is 7425 m/s, while the target value is set at 7482.2 m/s. When the model is simulated without a change in center of gravity, the velocity drops to 6603.8 m/s, resulting in an 11.06% deviation from the target. Similarly, without inertia changes, the velocity decreases to 6499.4 m/s, showing a 12.47% deviation. In the case of constant aerodynamics, the velocity further decreases to 6195.5 m/s, with a 16.56% deviation. The combined effect of all three cases results in a significant deviation, with the velocity decreasing to 4613.5 m/s, exhibiting a 37.87% difference from the target orbit velocity. For the γ parameter, the initial 6DOF result is −0.0074 degrees, aiming to align with a target of 0 degrees. Without a change in CG, γ increases to 21.8 degrees, deviating from the target. Similarly, without a moment of inertia change, γ becomes −8.54 degrees, showing a deviation. In the case of constant aerodynamics, γ increases even more to 27.41 degrees, with a substantial deviation. The combined effect of all three cases results in γ of 80.03 degrees, indicating a significant deviation from the target. Examining the h parameter, the initial 6DOF result is 747.6 km, with a target set at 741.2 km. Without a change in CG, the altitude increases to 1249.4 km, resulting in a 68.6% deviation from the target. Without inertia changes, the altitude decreases to 896.02 km, showing a 20.9% deviation. In the case of constant aerodynamics, the altitude further increases to 1546.61 km, with a substantial 108.7% deviation. The combined effect of all three cases results in a significant altitude increase to 2417.6 km, exhibiting a 226.2% difference from the target.

Table 10 presents results for the 6DOF model alongside target values and showcases the percentage differences for each specific modeling scenario for the original Minotaur-I launch vehicle (Northrop Grumman, West Falls Church, Virginia). Starting with the V parameter, the initial 6DOF result is 7460.2 m/s, with a target value of 7482.2 m/s.

When simulating without a change in CG, the velocity decreases to 6690.4 m/s, resulting in a 10.6% deviation from the target. Without a moment of inertia change, the velocity further decreases to 6301.3 m/s, showing a 15.8% deviation. In the case of constant aerodynamics, the velocity decreases even more to 6023.4 m/s, with a 19.5% deviation. The combined effect of all three cases results in a substantial drop in velocity to 4209.2 m/s, exhibiting a significant 43.7% difference from the target. For the γ parameter, the initial 6DOF result is 0.0052 degrees, aiming to align with a target of 0 degrees. Without a change in CG, γ increases to 16.5 degrees, deviating from the target value. Similarly, without a moment of inertia changes, γ becomes -6.9 degrees, showing a deviation. In the case of constant aerodynamics, γ increases even more to 31.8 degrees, with a substantial deviation. The combined effect of all three cases results in γ of 77.1 degrees, indicating a significant deviation from the target. Examining the h parameter, the initial 6DOF result is 743.7 km, with a target set at 741.2 km. Without a change in CG, the altitude increases to 1102.6 km, resulting in a 48.8% deviation from the target. Without a moment of inertia changes, the altitude decreases to 913.4 km, showing a 23.2% deviation. In the case of constant aerodynamics, the altitude further increases to 1325.9 km, with a substantial 78.9% deviation. The combined effect of all three cases results in a significant altitude increase to 2269.3 km, exhibiting a substantial 206.2% difference from the target. This detailed analysis highlights the diverse impacts of CG, moment inertia, and aerodynamic changes on the comprehensive modeling results. Therefore, it can be observed that comprehensive modeling leads to a critical difference in the optimization process, while in simulations without comprehensive modeling, the desired trajectory is achieved using different design parameters. For example, it is known that the flight path angle plays a dominant role in the trajectory of the launch vehicle, and the flight path angle is directed by the TVC angle. In this study, for instance, while the TVC angle of the first stage is sufficient for placing the payload on the target orbit in the 6DOF model when it is 4.882 degrees, in the 3DOF model, a different value from 4.882 degrees could be used to place the payload on the target orbit.

5. Discussion and Conclusions

In the present work, a multidisciplinary design optimization of a launch vehicle with a hybrid last stage was carried out and compared with the existing all-solid-stages launch vehicle, Minotaur-I, for performance improvements. The MDO problem is formulated to maximize the total impulse-to-weight ratio while satisfying target orbit parameters such as γ, h, and V criteria for a better I_{sp} value than the solid stage. Within the MDO process, the propulsion, aerodynamics, environment, and flight dynamics subsystems were modeled using MATLAB 2017b in a 6DOF simulation. The nonlinear coupling between subsystems was considered to address the research gap, making it possible to solve the complex optimization problem and determine the hybrid motor characteristics and various trajectory parameters, including the TVC angle, necessary to achieve the target orbit for a specified PM and mission. Aerodynamic coefficients were modeled using DATCOM v2011, while structural properties were obtained from CATIA V5R19. In the optimization process, all subsystems, including variations in length (L^*) and m, are updated in each iteration. This comprehensive optimization approach leads to the determination of the optimal solution.

Based on the results, the optimized design point 20245 achieves the target orbit more quickly compared to the reference trajectory. There are no significant changes in h of the first three stages. However, the decrease in V of the third stage during unpowered flight is smaller than in the optimized design due to the reduction in m_F resulting from the optimization process. It should be noted that the structural mass of the fourth stage remains the same as the reference to facilitate a comparison between the optimized propulsion system and the reference values. The value of γ initially starts near 90 degrees and gradually decreases using the optimized TVC angles, eventually approaching zero. The absolute errors in h and V are less than 1%, as expected.

According to the results in Table 6, the optimized design operates with lower T, shorter t_{burn}, higher I_{sp}, and a greater I_t/w_0. Despite the improvement, the optimized system is slightly longer in L^*. Although L^* of the stage and the total vehicle is increased, this L^* increase is not critical due to the updates in the subsystems considering the subsystem couplings during the optimization iterations. Consequently, any unfavorable conditions would have been observed in the optimization results, resulting in a limited number of feasible points. Overall, it can be concluded that the performance and efficiency of the launch vehicle are enhanced by incorporating a hybrid propulsion system.

The results also demonstrate that the optimized design reaches the target orbit faster, with a smaller V decrease during the unpowered flight of the third stage. As a result, the mission t and m consumption are reduced through the modification of the last stage with hybrid propulsion. The TVC angles of the first and last stages are also obtained to ensure they remain within the control deflection limits.

In addition, the comparison between the 3DOF and 6DOF models provided valuable insights. The 3DOF model lacks complex angular velocity calculations present in the 6DOF model, and it excludes essential factors like moment of inertia, center of mass, and moment changes. As the simulation progresses, the disparity between these two models widens. Specifically, the percentage differences between the 3DOF and 6DOF models were found to be 11.55% in velocity and 8.02% in altitude. While the 6DOF model closely aligns with the targeted parameters, there is evidence that the 3DOF model results deviate from the targeted parameters when run with the parameters entered into the 6DOF model.

Further analysis of the results for the hybrid last stage reveals significant differences when specific parameters are neglected. Neglecting changes in the center of gravity results in differences of 11.06% in velocity and 68.6% in altitude. Similarly, neglecting changes in the moment of inertia leads to differences of 12.47% in velocity and 20.9% in altitude. Assuming constant aerodynamic coefficients results in differences of 16.5% in velocity and 108.7% in altitude. In all these cases, the flight path angle deviates significantly from zero. Moreover, when all three cases are neglected, substantial differences of 37.87% in velocity and 226.2% in altitude are observed, with the flight path angle being notably different from zero. When conducting further analysis of the results for the original solid last stage, significant differences emerge when specific parameters are neglected. Neglecting changes in the center of gravity yields differences of 10.6% in velocity and 48.8% in altitude. Similarly, overlooking changes in moment of inertia results in differences of 15.8% in velocity and 23.2% in altitude. Assuming constant aerodynamic coefficients further produces differences of 19.5% in velocity and 78.9% in altitude. In all these cases, a noticeable trend is the significant deviation of the flight path angle from zero. Furthermore, neglecting all three cases leads to substantial differences of 43.7% in velocity and 206.2% in altitude, with the flight path angle notably diverging from zero. This highlights the critical impact of comprehensive modeling on the optimization process, whereas simulations without comprehensive modeling achieve the desired trajectory using different design parameters.

Consequently, it is seen that the performance of the launch vehicle is enhanced by utilizing a hybrid propulsion system, which offers lower production and manufacturing costs compared to other propulsion systems. The major contribution of the present work is considered to be the study of HRMs through the application of subsystems. Our future goal is to apply different parameters to the HRM system to better understand the relationship between environmental changes and HRMs.

Author Contributions: Conceptualization, U.A. and A.R.A.; Methodology, U.A. and U.D.G.; Investigation, U.A., A.R.A. and U.D.G.; Writing—original draft, U.A.; Writing—review & editing, A.R.A. and U.D.G.; Supervision, A.R.A.; Project administration, A.R.A. All authors have read and agreed to the published version of the manuscript.

Funding: This research has been supported by the ITU Coordinatorship of Scientific Research Projects, grant number MDK-2019-41839.

Institutional Review Board Statement: Not applicable.

Informed Consent Statement: Not applicable.

Data Availability Statement: The data presented in this study are available on request from the corresponding author. The data are not publicly available due to privacy.

Conflicts of Interest: Author Ukte Aksen was employed by the company Aselsan Inc. The remaining authors declare that the re-search was conducted in the absence of any commercial or financial relationships that could be construed as a potential conflict of interest.

References

1. Niederstrasser, C. SSC 18-IX-01 Small Launch Vehicles—A 2018 State of the Industry Survey. In Proceedings of the 32nd Annual AIAA/USU Conference on Small Satellites, Lagan, UT, USA, 4–9 August 2018. SSC18-IX-01.
2. VirginGalactic. SpaceShipOne. Available online: https://airandspace.si.edu/collection-objects/spaceshipone/nasm_A20050459000 (accessed on 26 September 2023).
3. ARCASpace. Arca Made Available the Ecorocket Technology for Civilian and Military Applications. Available online: https://www.arcaspace.com/ (accessed on 26 September 2023).
4. Messier, D. EXPACE Raises US$182 Million for Small Satellite Launchers. Parabolic Arc. 2020. Available online: https://web.archive.org/web/20201204225826/http://www.parabolicarc.com/2017/12/20/expace-raises-182-million-small-satellite-launchers/ (accessed on 26 September 2023).
5. Faenza, M.G.; Boiron, A.J.; Haemmerli, B.; Lennart, S.; Vesteras, T.; Verberne, O. Getting Ready for Space: Nammo's Development of a 30 kN Hybrid Rocket Based Technology Demonstrator. In Proceedings of the Nammo Raufoss AS, 7th European Conference for Aeronautics and Space Sciences, Milan, Italy, 3–6 July 2017.
6. Yonhap, S. Korean Startup Innospace Launches Test Launch Vehicle HANBIT-TLV. Available online: https://www.koreaherald.com/view.php?ud=20230320000109 (accessed on 20 March 2023).
7. Casalino, L.; Masseni, F.; Pastrone, D. Optimal Design of Hybrid Rocket Small Satellite Launchers Ground Versus Airborne Launch. *J. Spacecr. Rocket.* **2022**, *59*, 2084–2093. [CrossRef]
8. Casalino, L.; Masseni, F.; Pastrone, D. Deterministic and Robust Optimization of Hybrid Rocket Engines for Small Satellite Launchers. *J. Spacecr. Rocket.* **2021**, *58*, 1893–1903. [CrossRef]
9. Kitagava, Y.; Kitagava, K.; Nakamiya, M. Multi-Stage Hybrid Rocket Conceptual Design for Micro-Satellites Launch using Genetic Algorithm. *Trans. Jpn. Soc. Aeronaut. Space Sci.* **2012**, *55*, 229–236. [CrossRef]
10. Rao, D.; Cai, G.; Zhu, H.; Tian, H. Design and optimization of variable thrust hybrid rocket motors for sounding rockets. *Sci. China Technol. Sci.* **2012**, *55*, 125–135. [CrossRef]
11. Glaser, C.; Hijlkema, J.; Anthoine, J. Bridging the Technology Gap: Strategies for Hybrid Rocket Engines. *Aerospace* **2023**, *10*, 901. [CrossRef]
12. Lu, P.; Pan, B. Trajectory optimization and guidance for an advanced launch system. In Proceedings of the 10th Aerospace Sciences Meeting and Exhibit, Reno, NV, USA, 9 January 1992.
13. Gath, P.F.; Calise, A.J. Optimization of Launch Vehicle Ascent Trajectories with Path Constraints and Coast Arcs. *J. Guid. Control Dyn.* **2001**, *24*, 296–304. [CrossRef]
14. Miele, A. Multiple-Subarc Gradient-Restoration Algorithm, Part 1: Algorithm Structure. *J. Optim. Theory Appl.* **2003**, *116*, 1–17. [CrossRef]
15. Bayley, D. Design Optimization of Space Launch Vehicles Using a Genetic Algorithms. *J. Spacecr. Rocket.* **2007**, *45*, 733–740. [CrossRef]
16. Lappas, V. Trade-Offs and Optimization of Air-Assisted Launch Vehicles for Small Satellites. *J. Small Satell.* **2019**, *7*, 753–772.
17. Schoettle, U.M.; Hillesheimer, M. Performance optimization of an airbreathing launch vehicle by a sequential trajectory optimization and vehicle design scheme. In Proceedings of the Navigation and Control Conference, New Orleans, LA, USA, 12–14 August 1991. [CrossRef]
18. Miele, A. Multiple-Subarc Gradient-Restoration Algorithm, Part 2: Application to a Multistage Launch Vehicle Design. *J. Optim. Theory Appl.* **2002**, *116*, 19–39. [CrossRef]
19. Rafique, A.F.; LinShu, H.; Zeeshan, Q.; Kamran, A.; Nisar, K.; Xioawei, W. Hybrid Optimization Method for Multidisciplinary Design of Air Launched Satellite Launch Vehicle. In Proceedings of the 45th AIAA/ASME/SAE/ASEE Joint Propulsion Conference and Exhibit, Denver, CO, USA, 2–5 August 2009. [CrossRef]
20. Wiegand, A.; Cremaschi, F.; Winter, S.; Weikert, S.; Link, T.; Zell, D.; Albinger, J. *Design Optimisation and Performance Analysis of Launch Vehicles with ASTOS*; Deutsche Gesellschaft für Luft-und Raumfahrt-Lilienthal-Oberth eV: Bonn, Germany, 2015.
21. Mall, K.; Taheri, E. 3-DOF Reentry Trajectory Optimization for a Reusable Launch Vehicle Using an Advanced Indirect Method. *J. Spacecr. Rocket.* **2022**, *59*, 1463–1474. [CrossRef]
22. Villanueva, F.M. Small Modular Launch Vehicle Multidisciplinary Design Optimization. In Proceedings of the IEEE Aerospace Conference (AERO), Big Sky, MT, USA, 5–12 March 2022.
23. Eberhart, R.C.; Shi, Y. Comparison Be-tween Genetic Algorithms and Particle Swarm Optimization. *Evol. Program. VII Lect. Notes Comput. Sci.* **1998**, *1447*, 611–616.
24. Venter, G.; Sobieszczanski-Sobieski, J. Particle Swarm Optimization. *AIAA J.* **2003**, *41*, 1583–1589. [CrossRef]

25. Pontani, M. Particle swarm optimization of as-cent trajectories of multistage launch vehicles. *Acta Astronaut.* **2014**, *94*, 852–864. [CrossRef]
26. Dileep, M.V.; Kamath, S.; Nair, V.G. Particle Swarm Optimization Applied to Ascent Phase Launch Vehicle Trajectory Optimization Problem. *Procedia Comput. Sci.* **2015**, *54*, 516–522. [CrossRef]
27. Zhou, H.; Wang, X.; Bai, Y.; Cui, N. Ascent phase trajectory optimization for vehicle with mul-ti-combined cycle engine based on improved particle swarm optimization. *Acta Astronaut.* **2017**, *140*, 156–165. [CrossRef]
28. Dukeman, G.A. Atmospheric Ascent Guidance for Rocket-Powered Launch Vehicles. In *AIAA Guidance, Navigation, and Control Conference and Exhibit*; American Institute of Aeronautics and Astronautics: Monterey, CA, USA, 2002.
29. Wang, Z.; Wu, Z. Six-DOF Trajectory Optimization for Reusable Launch Vehicles via Gauss Pseudospectral Method. *J. Syst. Eng. Electron.* **2016**, *27*, 434–441. [CrossRef]
30. Rao, P.P.; Sutter, B.M.; Hong, P.E. Six-Degree-of-Freedom Trajectory Targeting and Optimization for Titan Launch Vehicles. *J. Spacecr. Rocket.* **1997**, *34*, 341–346. [CrossRef]
31. Li, Y.; Pang, B.; Wei, C.; Cui, N.; Liu, Y. Online Trajectory Optimization for Power System Fault of Launch Vehicles via Convex Programming. *J. Aerosp. Eng.* **2020**, *98*, 105682. [CrossRef]
32. Calise, A.J.; Brandt, N. Generation of Launch Vehicle Abort Trajectories Using a Hybrid Optimization Method. *J. Guid. Control Dyn.* **2004**, *27*, 929. [CrossRef]
33. Brown, N.F.; Olds, J.R. Evaluation of Multidisciplinary Optimization Techniques Applied to a Reusable Launch Vehicle. *J. Spacecr. Rocket.* **2006**, *43*, 1289–1300. [CrossRef]
34. Rafique, A.F.; He, L.; Kamran, A.; Zeeshan, Q. Hyper Heuristic Approach for Design and Optimization of Satellite Launch Vehicle. *Chin. J. Aeronaut.* **2011**, *24*, 150–163. [CrossRef]
35. Rea, J. Launch Vehicle Trajectory Optimization Using a Legendre Pseudospectral Method. In *AIAA Guidance, Navigation, and Control Conference and Exhibit*; American Institute of Aeronautics and Astronautics: Austin, TX, USA, 2003.
36. Orbital Sciences. *Minotaur I Space Launch Vehicle-Fact Sheet*; NASA: Washington, DC, USA, 2006; Retrieved 15 June 2021.
37. Williams, J.E.; Vukelich, S.R. *The USAF Stability and Control Digital DATCOM. Volume I. User's Manual*; Tech. Rep. AFFDL-TR-79-3032 Volume I; Air Force Flight Dynamics Laboratory (AFFDL): Greene County, OH, USA, 1979.
38. DassaultSyst'emes. CATIA. Available online: https://www.3ds.com/products-services/catia/ (accessed on 26 September 2023).
39. Carpenter Technology. *Titanium Alloy 6Al-4V Technical Data Sheet*; Carpenter Technology: Philadelphia, PA, USA, 2000.
40. Nyamekye, P.; Rahimpour Golroudbary, S.; Piili, H.; Luukka, P.; Kraslawski, A. Impact of additive manufacturing on titanium supply chain: Case of titanium alloys in automotive and aerospace industries. *Adv. Ind. Manuf. Eng.* **2023**, *6*, 100112. [CrossRef]
41. Pavlis, N.K.; Holmes, S.A.; Kenyon, S.C.; Factor, J.K. The development and evaluation of the Earth Gravitational Model 2008 (EGM2008). *J. Geophys. Res. Solid Earth* **2012**, *117*. [CrossRef]
42. Markley, F.L.; Crassidis, J.L. *Fundamentals of Spacecraft Attitude Determination and Control*; Springer: Berlin/Heidelberg, Germany, 2014; pp. 385–388.
43. *NOAA-SIT 76-1562*; NOAA, NASA, and USAF, U.S. Standard Atmosphere 1976. National Oceanic and Amospheric Administration: Silver Spring, MD, USA, 1976.
44. Zhu, H.; Wang, P.; Xu, W.; Zhang, Y.; Tian, H.; Cai, G. Design Optimization and Parameter Analysis of a Hybrid Rocket Motor-Powered Small LEO Launch Vehicle. *Int. J. Aerosp. Eng.* **2021**, *2021*, 5574436. [CrossRef]
45. Tianfang, W.; Guobiao, C.; Hui, T.; Hao, Z.; Yuanjun, Z.; Xintong, L. Optimization design in single wagon-wheel fuel grain of hybrid rocket motor. *FirePhysChem* **2021**, *1*, 212–221. [CrossRef]
46. Sutton, G.P.; Biblarz, O. Rocket Propulsion Elements, New York. 2001. Available online: https://ftp.idu.ac.id/wp-content/uploads/ebook/tdg/DESIGN%20SISTEM%20DAYA%20GERAK/Rocket%20Propulsion%20Elements.pdf (accessed on 26 September 2023).
47. MathWorks. Matlab. Available online: https://www.mathworks.com/?stid=gnlogo (accessed on 26 September 2023).
48. Stevens, B.L.; Lewis, F.L.; Johnson, E.N. *Aircraft Control and Simulation Dynamics, Controls Design and Autonomous Systems*, 3rd ed.; Wiley: Hoboken, NJ, USA, 2016; Volume 36, p. 54.
49. Christodoulou, N.S. An Algorithm Using Runge-Kutta Methods of Orders 4 and 5 for Systems of ODEs. *Int. J. Numer. Methods Appl.* **2009**, *2*, 47–57.
50. Kennedy, J.; Eberhart, R. Particle swarm optimization. In Proceedings of the IEEE International Conference on Neural Networks, Perth, Australia, 27 November–1 December 1995; pp. 1942–1948.
51. Lalwani, S.; Sharma, H.; Satapathy, S.C.; Deep, K.; Bansal, J.C. A Survey on Parallel Particle Swarm Optimization Algorithms. *Arab. J. Sci. Eng.* **2019**, *44*, 2899–2923. [CrossRef]
52. Depince, P.; Guedas, B.; Picard, J. Multidisciplinary and multiobjective optimization: Comparison of several methods. In Proceedings of the 7th World Congress on Structural and Multidisciplinary Optimization, Seoul, Republic of Korea, 21–25 May 2007.
53. Chen, H. Multidisciplinary Design Optimization (MDO). In *Encyclopedia of Ocean Engineering*; Springer: Singapore, 2020; pp. 1–7. [CrossRef]
54. Peri, D.; Dessi, D.; Campana, E. Global Optimization Algorithms in Multidisciplinary Design Optimization. In Proceedings of the 12th AIAA/ISSMO Multidisciplinary Analysis and Optimization Conference, MAO, Victoria, BC, Canada, 10–12 September 2008. [CrossRef]

55. Buckley, S.J.; Weis, S.C.; Schoneman, S. The Orbital/Suborbital Program (OSP) Minotaur Space Launch Vehicle: Using Surplus ICBM Motors to Achieve Low Cost Space Lift For Small Satellites. In Proceedings of the 12th AIAA/USU Conference on Small Satellites, Long Beach, CA, USA, 19–21 September 2000. [CrossRef]
56. OrbitalATK. *Minotaur I User's Guide*; Tech. Rep.; OrbitalATK: Dulles, VI, USA, 2015.
57. ESTECO. ModeFrontier. Available online: https://engineering.esteco.com/modefrontier/ (accessed on 26 September 2023).
58. Zhang, F.; Litson, K.; Feldon, D.F. Social predictors of doctoral student mental health and well-being. *PLoS ONE* **2022**, *17*, e0274273. [CrossRef]
59. Pundziene, A.; Sermontyte-Baniule, R.; Rialp-Criado, J.; Chesbrough, H. Indirect effect of open innovation on clinical and economic value creation in digital healthcare: A comparative study of European countries. *J. Bus. Res.* **2023**, *159*, 113701. [CrossRef]
60. Brochu, R.; Lestage, R. *Three-Degree-of-Freedom (DOF) Missile Trajectory Simulation Model and Comparative Study with a High Fidelity 6DOF Model*; DRDC Valcartier TIM: Quebec City, QC, Canada, 2003.